# On OFDM in Doubly-Dispersive Channels

A Thesis

Presented in Partial Fulfillment of the Requirements for

the Degree Master of Science in the

Graduate School of The Ohio State University

By

Siddharth D'Silva, B.E.

* * * * *

The Ohio State University

2002

Master's Examination Committee:

Dr. Philip Schniter, Adviser

Dr. Oscar Takeshita

Approved by

Adviser

Department of Electrical Engineering

# ABSTRACT

It is a well known fact that orthogonal frequency division multiplexing (OFDM) provides a practical solution to counter the intersymbol interference (ISI) problem imposed by the frequency-selective fading (FSF) channel. While the application of OFDM in slow-FSF multipath channels is well understood, the application of OFDM in fast-FSF multipath channels is fraught with several difficulties, many of which have not been practically treated in the literature. We premise our work on the claim that current trends in broadband wireless communication systems dictate that channel time-variation will soon play an important role in OFDM systems. The primary advantages of cyclic prefix OFDM in time-invariant FSF channels, i.e., the absence of ISI and of intercarrier interference (ICI), do not carry over to time- and frequency-selective, i.e., doubly-selective channels. As a result, the standard zero-forcing (ZF), linear minimum mean-square error (LMMSE) and maximum likelihood (ML) detection techniques become prohibitively complex.

An analytic study of the nature of ICI shows that it is most prominent among nearby subcarriers. Further, incorporating the effects of distant-subcarrier-ICI might improve the detection performance but would prevent practical implementation. As

a practical suboptimal alternative, we propose a low-complexity linear receiver pre-processing scheme that renders the ICI response sparse, thereby simplifying subsequent symbol detection. The ICI structure suggests pre-processing that strives to limit the ICI to *adjacent* subcarriers.

Finally we propose computationally-efficient suboptimal decision-feedback strategies to obtain reliable soft-symbol estimates which can be fed to a decoder. Simulation results indicate good performance relative to the standard detectors but with significant computational savings.

# On OFDM in Doubly-Dispersive Channels

By

Siddharth D'Silva, M.S.

The Ohio State University, 2002

Dr. Philip Schniter, Adviser

It is a well known fact that orthogonal frequency division multiplexing (OFDM) provides a practical solution to counter the intersymbol interference (ISI) problem imposed by the frequency-selective fading (FSF) channel. While the application of OFDM in slow-FSF multipath channels is well understood, the application of OFDM in fast-FSF multipath channels is fraught with several difficulties, many of which have not been practically treated in the literature. We premise our work on the claim that current trends in broadband wireless communication systems dictate that channel time-variation will soon play an important role in OFDM systems. The primary advantages of cyclic prefix OFDM in time-invariant FSF channels, i.e., the absence of ISI and of intercarrier interference (ICI), do not carry over to time- and frequency-selective, i.e., doubly-selective channels. As a result, the standard zero-forcing (ZF), linear minimum mean-square error (LMMSE) and maximum likelihood (ML) detection techniques become prohibitively complex.

An analytic study of the nature of ICI shows that it is most prominent among nearby subcarriers. Further, incorporating the effects of distant-subcarrier-ICI might improve the detection performance but would prevent practical implementation. As a practical suboptimal alternative, we propose a low-complexity linear receiver pre-processing scheme that renders the ICI response sparse, thereby simplifying subsequent symbol detection. The ICI structure suggests pre-processing that strives to limit the ICI to *adjacent* subcarriers.

Finally we propose computationally-efficient suboptimal decision-feedback strategies to obtain reliable soft-symbol estimates which can be fed to a decoder. Simulation results indicate good performance relative to the standard detectors but with significant computational savings.

Dedicated to my parents Philo and Harry D'Silva, my sister Shalini and the lovely Ms. Audrey Braganza

# ACKNOWLEDGMENTS

My two years at the Ohio State University have been a great learning experience, both academic and otherwise. I take this opportunity to thank the institution and all the wonderful people I've come to know through my stay at OSU.

First and foremost, I would like to thank my graduate advisor, Prof. Philip Schniter, for his patience and timely advice. I will always cherish Phil as a friend and guide who gave me good constructive feedback and taught me to work smart and play hard. I would like to thank Prof. Oscar Takeshita for being a part of my Master's examination committee. Many thanks also go to Profs. Hesham El-Gamal, Randy Moses and Lee Potter for their advice, insightful comments and teaching.

Next, I would like to thank my colleagues at the Information Processing Systems (IPS) laboratory for their friendship and good spirit. I want to thank Ravi for providing excellent technical support to the IPS lab; Defne, Emre, Jing and Xiaoxia for their help and advice on research and for being inspiring senior lab members and the amicable Ulku for her alacrity.

I would also like to thank (alphabetically) Reetesh, Samrat, Sathish, Shalini, Sukirti and Tathagatha for being a part of my numerous extracurricular activities.

Saving the best for last, I would like to thank Adam and Ruth for being exemplary friends who were always there for me, and my closest friends at OSU, Bijoy and Amol, for the fun times we had with classes, discussing research, the bar & club scenes, the

picnics, the camping trips, the road trips, the Hindi banter and all the Indian cooking that made my stay in the US a memorable one.

# VITA

| | |
|---|---|
| April 22, 1979 | Born - Madras, India |
| Summer 2000 | B.E. Electronics Engineering, Sardar Patel College of Engineering, Bombay |
| Fall 2000 - Summer 2001 | Graduate Teaching Associate, The Ohio State University. |
| Fall 2001- Fall 2002 | Graduate Research Associate, The Ohio State University |

# PUBLICATIONS

Philip Schniter and Siddharth D'Silva, "Low-Complexity Detection of OFDM in Doubly-Dispersive Channels". *Proc. 36th Asilomar Conference on Signals, Systems and Computers*, (Pacific Grove, CA), Nov. 2002.

# FIELDS OF STUDY

Major Field: Electrical Engineering

Studies in:

| | |
|---|---|
| Detection & Estimation Theory, Digital Signal Processing, Adaptive Filtering | Prof. Philip Schniter |
| Communication Theory, Coding Theory | Prof. Hesham El-Gamal |

# TABLE OF CONTENTS

# LIST OF FIGURES

# CHAPTER 1

# INTRODUCTION

Broadband wireless communication is an important component of the evolving global information infrastructure. Current and future generation wireless links are expected to provide high data rate transmission of multimedia services such as wireless video, wireless Internet access and mobile computing, and in some cases are expected to do so in very high mobility situations [1]. At the same time, our limited radio spectrum has become an increasingly precious resource, entailing high spectral efficiency, the use of higher carrier frequencies and in some cases spectrum sharing between different wireless users. In addition, consumer demands dictate that the cost of wireless terminals be kept low and their sizes small. Thus wireless communication technology of the future must operate at high data rates, at high carrier frequencies, in high mobility situations and under high levels of spectral interference, all while maintaining reliable data transmission using small and inexpensive components.

## 1.1 Problems Inherent to Broadband Wireless Communication

In wireless communication, an information signal with a particular bandwidth is modulated to a designated frequency band for transmission. A digital communication

signal can be viewed as a sequence of pulses having period $T$. High data rate applications necessitate the use of short pulses (e.g., $T \leq 1\mu$s) and hence large bandwidth ($B = 1/T \geq 1$ MHz), or broadband signals.

Many modern broadband wireless systems employ carrier signals at frequencies in the range of several GHz, leading to a transmitted-signal wavelength on the order of millimeters. Such high frequencies are used because lower frequencies have been reserved for pre-existing communication systems. Also, higher frequencies allow more significant frequency re-use: because high frequency signals are easily attenuated by buildings, trees and atmospheric impediments allowing the same frequency range to be used by a sufficiently distant, different wireless system. A high-frequency carrier coupled with a broadband information signal, poses significant challenges which can be understood by considering the signal propagation path between the transmit and receive antennas. Apart from a direct "line-of-sight" signal component between antennas (which arises in certain special circumstances), the received signal consists of a multitude of transmit-signal reflections from physical objects (or scatterers) in the vicinity of the antennas. Typical scatterers are buildings, trees, cars and the pavement. Each scattering path can be characterized by an attenuation, phase-shift and delay. These values are a function of the reflectivity of the scatterer and the total length of the reflected path. The reflected signals may combine constructively or destructively at the receive antenna, depending on their relative phase, resulting in an amplification or annihilation of the transmitted signal. (180° phase difference yields complete cancellation.)

For signals in the GHz frequency range, path-length differences on the order of millimeters can cause significant phase differences and thus major fluctuations in the

received signal level. This implies that even wind-induced antenna and/or tree-leaf movements in "fixed" wireless applications can produce severe signal fades. This "multipath-fading" makes it difficult to reliably recover the transmitted information when the received signal level falls below the noise/interference level, and thus presents a fundamental challenge to wireless data communication.

When the antennas or the dominant scatterers are mobile, the relative scatterer locations may change drastically over short periods of time, leading to a rapid change in signal level, or rapid fading. The "fading-rate" is then proportional to the relative speed between scatterers and antennas.

The fading mechanism described above, called "flat-fading", applies to any signal (narrowband or broadband) that is transmitted at high frequencies. An additional fading mechanism is inherent to broadband signals. Say $T$ is small compared to the path delay differences. Then the receive antenna might observe one pulse (or data symbol) across a short-delay (e.g., line of sight) path and simultaneously observe previously-transmitted pulses across long-delay (e.g., distant scatterer) paths. Thus the received signal is not only plagued by the signal fading described above but also by inter-symbol interference (ISI): Each symbol observation is corrupted by echos of previously transmitted symbols. In fact, many broadband[1] applications have $\geq$100 different symbols interfering at any given time. Again, these symbols may combine constructively or destructively, depending on the data values they represent, leading to potential signal cancellation. The arrival of multiple delayed paths acts like a filter on the transmitted symbol sequence, i.e., we expect some frequencies within the

[1] "Narrowband" signals are characterized by pulse (symbol) durations that are large compared to the path delay differences, thus avoiding interference of pulses at the receiver.

transmitted-signal bandwidth to be attenuated more than others. For this reason, this latter fading is known as "frequency-selective fading[2]".

While at first ISI might seem as a serious impediment that wireless system designers have to contend with, the presence of severe ISI actually offers the possibility of frequency-diversity gain afforded by the seemingly random nature of multipath fading [2,3]. The optimal sequence detector (the maximum-likelihood detector) required to fully exploit this diversity gain is prohibitively complex as its complexity is an exponential function of the channel memory length. Thus, in practice, ISI-challenged systems employ time-domain equalization [4] which, while suboptimal from a detection standpoint, reasonably exploits the diversity offered by the multipath channel. The time-domain equalizer (TDE) attempts to adaptively invert the filtering action of the channel. It should be noted that as ISI increases, computing the TDE coefficients becomes computationally intensive making it an infeasible alternative. Realizing that the time-domain filtering (convolution) mentioned above is equivalent to multiplication of the spectra of the signals involved, frequency-domain equalization (FDE) was suggested in [5,6]. While FDE complexity is independent of the size of channel memory, it requires a block transmission of symbols with a sufficiently large guard interval and also assumes the presence of a constant channel over the block duration.

## 1.2 OFDM, a Practical Alternative

A more practical solution to the severe ISI problem is given by a multicarrier modulation scheme known as orthogonal frequency division multiplexing (OFDM) [7–9].

[2]In contrast, flat fading affects all the frequency components within the transmitted-signal band equally.

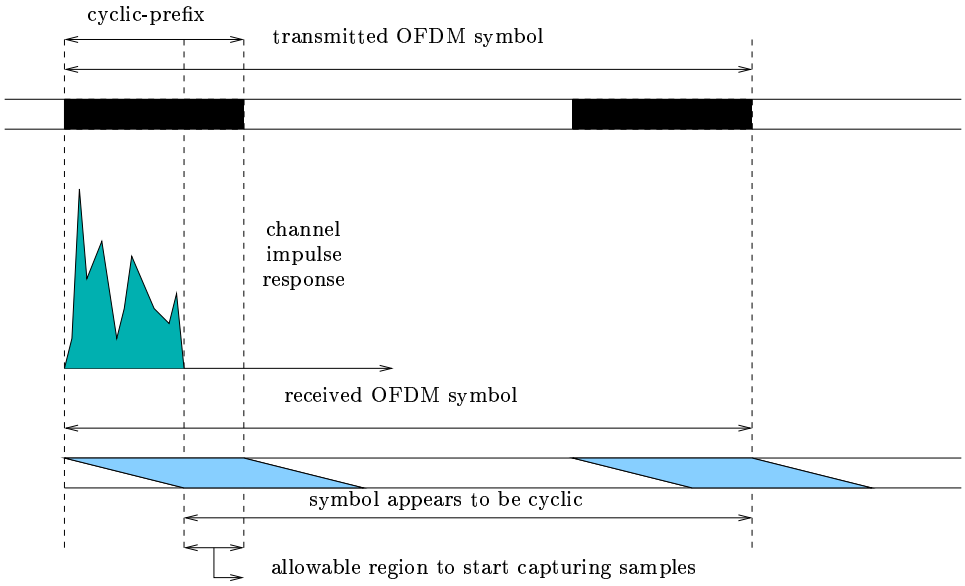


Figure 1.1: Example of an OFDM symbol transmitted on a multipath channel

Here, broadband data is transmitted using a large number of parallel low-rate (narrowband) streams called "subcarriers" whose symbol periods are large compared to the channel delay spread. Thus the subcarriers experience flat (rather than frequency-selective) fading, avoiding ISI and hence greatly simplifying receiver design. Modulation and demodulation of the subcarriers can be accomplished in a block-by-block fashion using the computationally-efficient fast Fourier transform (FFT) algorithm, making OFDM transceiver implementation practical. An important detail is that a guard interval of duration greater than the channel delay spread must be inserted between transmitted blocks to make them cyclic and ensure subcarrier orthogonality which is the key to receiver simplicity. The OFDM guard interval leads to a slight loss in efficiency, although this loss can be made negligible by increasing the size of

the OFDM block. Thus at first glance, OFDM seems to offer an efficient solution to current broadband wireless communication problems.

The operation of OFDM described above requires that the fading rate is slow enough (slow time variation over the OFDM block) to keep the subcarriers orthogonal. As the fading rate increases, a subcarrier experiences a fading gain that varies significantly along the OFDM block leading to an increase in the subcarrier bandwidth which is proportional to the fading rate. This phenomenon, known as "Doppler-spreading" causes OFDM subcarriers to interfere with one another, a phenomenon called intercarrier interference (ICI) which can severely affect the receiver's detection performance if neglected. In Section 2.2 we show that, for channels that exhibit fast time-selective fading, the loss of subcarrier orthogonality manifests as significant ICI. Thus, the primary advantage of OFDM in frequency-selective channels, namely the absence of ISI and of ICI, does not carry over to time- and frequency-selective channels.

Most current applications of OFDM operate under slow-fading conditions for which intra-symbol channel variation can be ignored, so that the ICI problem does not arise. However, time-selectivity cannot be ignored in the design of future broadband wireless systems. As mentioned above, future systems are likely to operate at very high carrier frequencies (i.e., $\geq$ 1GHz) and Doppler spread, an indicator of fading rate, is linearly proportional to carrier frequency [10]. In other words, effective rates of channel variation for a fixed mobile speed increase. Secondly, future wireless systems are bound to operate in very high mobility situations ($v > 200$ km/h), such as between high-speed cars/trains to "info-stations" placed along the vehicle's path [11], and Doppler spread is linearly proportional to vehicle speed [10]. Third, there is

a desire to minimize the capacity lost by insertion of the redundant OFDM guard interval. As traditional OFDM design specifies a guard length of at least the channel delay spread, redundancy can diminished through an increase in OFDM symbol duration. But, by increasing the OFDM symbol duration, the system becomes more sensitive to intra-block channel variation. Thus we can conclude that future broadband wireless applications will face channels that are significantly time-selective as well as frequency-selective.

## 1.3 Thesis Organization

This thesis has been organized into seven chapters. In Chapter 2 we provide an overview of wireless channel models, describe the basic OFDM system, and give a brief description of the existing work on OFDM in doubly-selective channels. In Chapter 3 we analyze and quantify the effect of a doubly-selective fading channel on OFDM, namely ICI, and in Chapter 4 we propose low-complexity linear receiver pre-processing that renders the ICI response sparse[3]. In Chapter 5 we review possible schemes for symbol detection and propose computationally-efficient decision-feedback soft-symbol estimation strategies that exploit the sparse ICI response. Simulation results in Chapter 6 clearly indicate good performance of the proposed sub-optimal schemes relative to the standard detection techniques but with significant computational savings. Finally in Chapter 7 we conclude our work and offer insights into the avenues for future work.

[3]This can be regarded as the frequency-domain dual of ISI-channel shortening that has been proposed to reduce the complexity of maximum likelihood sequence detection in single carrier systems [12].

# CHAPTER 2

# BACKGROUND

## 2.1 Wireless Channel Models

The wireless channel can be viewed as a "black box" placed between the transmitter and receiver of a communication system. Systems experiencing frequency-selective fading channels, model this black box as a random linear time-invariant (LTI) filter and summarize its characteristics by a discrete-time finite impulse response (FIR) $h(m), \quad m = 0, \ldots, N_h - 1$, where $N_h$ denotes the maximum delay spread of the channel in baud. As explained in Chapter 1, future broadband wireless applications will face channels that are significantly time- and frequency-selective. Thus, in this thesis, we adopt a more general approach to channel modeling and view the wireless channel as a random linear time-variant (LTV) filter characterized by one of the following four system models.

1. **Time-lag model**

   The time-lag model, better known as the impulse response of a LTV channel, can be denoted by $h_{t,l}(n, m), \quad n \in \mathbb{Z}, m = 0, \ldots, N_h - 1$. Here $h_{t,l}(n, m)$ specifies the output of the channel at time index-$n$ to a Kronecker delta applied

at time index-$(n-m)$. In an OFDM system we impose the additional constraint $n = 0, \ldots, N-1$. More explanation will be given in Section 2.2.

2. **Time-frequency model**

   This is a time-varying frequency response parameterization of the LTV channel. We denote it (non-sampled) by $H_{t,f}[n, \omega), \quad n \in \mathbb{Z}, \omega \in [0, 2\pi)$ where,

$$H_{t,f}[n, \omega) := \frac{1}{\sqrt{N}} \sum_m h_{t,l}(n, m) e^{-j\omega m}. \tag{2.1}$$

   Here $N$ is the length of the observation interval in time (i.e., $n = 0, \ldots, N-1, \ N \geq N_h$). We can also parameterize the system in terms of its sampled time-varying frequency response $h_{t,f}(n, k), \quad k = 0, \ldots, N-1$

$$h_{t,f}(n, k) := \frac{1}{\sqrt{N}} \sum_m h_{t,l}(n, m) e^{-j\frac{2\pi k}{N} m}. \tag{2.2}$$

3. **Doppler-lag model**

   This form of system parameterization is of particular interest for channels which are both delay and Doppler-spread limited as it enables a sparse yet complete representation of the channel. We denote the non-sampled Doppler-lag response by $H_{d,l}(\phi, m], \quad \phi \in [0, 2\pi), \ \ m = 0, \ldots, N_h - 1$

$$H_{d,l}(\phi, m] := \frac{1}{\sqrt{N}} \sum_n h_{t,l}(n, m) e^{-j\phi n} \tag{2.3}$$

   where again we have restricted $n = 0, \ldots, N-1$. We can also parameterize the system in terms of its sampled Doppler-lag response $h_{d,l}(\nu, m)$, $\nu = 0, \ldots, N-1$

$$h_{d,l}(\nu, m) := \frac{1}{\sqrt{N}} \sum_n h_{t,l}(n, m) e^{-j\frac{2\pi \nu}{N} n} \tag{2.4}$$

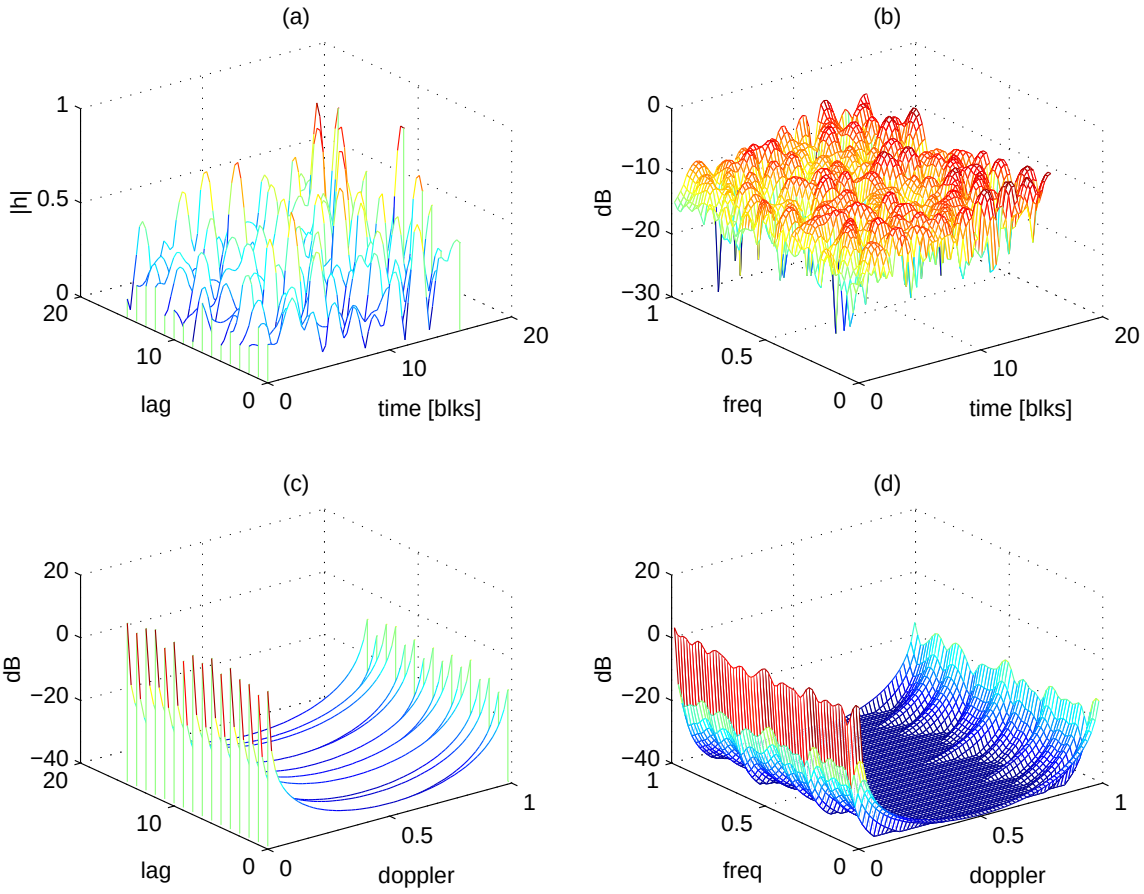


Figure 2.1: Example time-variant channel transmission functions

4. **Doppler-frequency model**

   This model is extensively used in this thesis to characterize the channel response at the OFDM receiver. It is denoted (non-sampled) by $H_{d,f}(\phi,\omega)$, $\phi,\omega \in [0,2\pi)$ where, using (2.1) and (2.3)

$$\begin{aligned} H_{d,f}(\phi,\omega) &:= \frac{1}{\sqrt{N}}\sum_m H_{d,l}(\phi,m]e^{-j\omega m} \\ &= \frac{1}{N}\sum_m\sum_n h_{t,l}(n,m)e^{-j\phi n}e^{-j\omega m} \end{aligned} \tag{2.5}$$

   From (2.2) and (2.4) we can also define the sampled Doppler-frequency response $h_{d,f}(\nu,k)$, $\nu,k = 0,\ldots,N-1$

$$h_{d,f}(\nu,k) := \frac{1}{N}\sum_m\sum_n h_{t,l}(n,m)e^{-j\frac{2\pi k}{N}n}e^{-j\frac{2\pi\nu}{N}m} \tag{2.6}$$

All the sampled transmission functions defined above are $N$-periodic in the Doppler and frequency indices $\nu$ and $k$. Note that the subscripts on each of the transmission function are used to denote the time/lag and Doppler/frequency interpretation of its two arguments. Fig. 2.1 gives an example of a time-varying channel represented by the four transmission functions defined above.

## 2.2 The OFDM system model

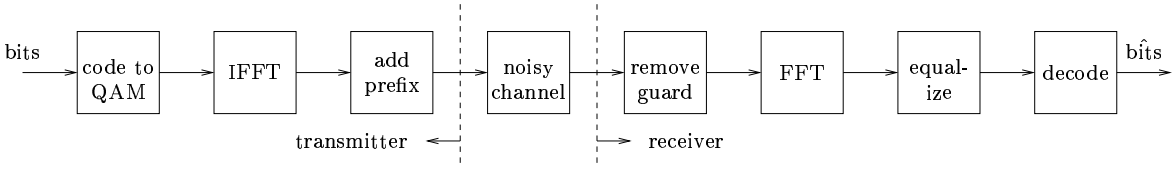


Figure 2.2: OFDM block diagram

To aid our discussion of OFDM behavior in fading wireless channels, we outline a system model to convey the main concepts. See Fig. 2.2 for an illustration.

In an OFDM system, each block of data contains information from $N$-frequency-domain symbols $\{s_k^{(i)}\}_{k=0}^{N-1}$ drawn from a $M$-QAM alphabet. Here $i$ denotes the OFDM block index and $M$ denotes the size of the QAM alphabet. The $k^{th}$ frequency-domain symbol is used to modulate a cyclically-prepended inverse Fourier transform (IDFT) basis vector, so that a sampled version of the time-domain transmitted signal $\{x^{(i)}(n)\}_{n=-N_p}^{N-1}$ for the $i^{th}$ block is given by

$$x^{(i)}(n) = \frac{1}{\sqrt{N}} \sum_{k=0}^{N-1} s_k^{(i)} e^{j\frac{2\pi n}{N}k} \tag{2.7}$$

where $N_p$ ($N_p \leq N$) denotes the length of the cyclic-prefix (guard interval). To prevent inter-block interference at the receiver and to ensure a circular (rather than linear) convolution with the channel response, the time-domain blocks are cyclically prepended with a prefix length $N_p$ of at least the channel impulse response length. The time-domain blocks are then serially transmitted through a multipath fading channel.

Assume that the time-domain received signal $r^{(i)}(n)$ is a noise corrupted and linearly distorted version of $x^{(i)}(n)$ as a consequence of a LTV channel with impulse response $h_{t,l}^{(i)}(n,m)$. Here $h_{t,l}^{(i)}(n,m)$ specifies the output of the system at time index $n$ within the $i^{th}$ block to a Kronecker delta applied at time index $(n-m)$. The channel is assumed to change continuously within a block (i.e., over $n$) as well as between blocks (i.e., over $i$). This time-lag block-indexed channel response can be related to

the general time-lag channel response $h_{t,l}(\tilde{n}, m)$ defined in Section 2.1 as

$$\begin{aligned} h_{t,l}(\tilde{n}, m) &= h_{t,l}^{\left(\left\lfloor \frac{\tilde{n}+N_p}{N+N_p} \right\rfloor\right)} \left( \langle \tilde{n} + N_p \rangle_{N+N_p} - N_p), m \right), \quad \tilde{n} \in \mathbb{Z} \\ h_{t,l}^{(i)}(n, m) &= h_{t,l}(i(N+N_p)+n, m), \quad i \in \mathbb{Z}, n \in \{-N_p, \ldots, N-1\} \end{aligned}$$

If the channel is causal with a maximum impulse response duration $N_h$, where $N_h \leq N_p \leq N$, then

$$r^{(i)}(n) = \sum_{m=0}^{N_h-1} h_{t,l}^{(i)}(n, m) x^{(i)}(n-m) + \tilde{w}_n^{(i)}, \quad n \in \{0, \ldots, N-1\} \tag{2.8}$$

The adequate length of the cyclic prefix enables the values of $x^{(i)}(n-m)$ in (2.8) to be well defined. We assume that $\tilde{w}_n^{(i)}$ are zero-mean white and Gaussian with variance $\sigma_w^2$. At each block $i$, the receiver drops the samples corresponding to the cyclic-prefix and applies $\{r^{(i)}(n)\}_{n=0}^{N-1}$ to a discrete Fourier transform (DFT), yielding $\{y_\nu^{(i)}\}_{\nu=0}^{N-1}$

$$y_\nu^{(i)} = \frac{1}{\sqrt{N}} \sum_{n=0}^{N-1} r^{(i)}(n) e^{-j\frac{2\pi\nu}{N}n} \tag{2.9}$$

It is convenient to extend the definition of $y_\nu^{(i)}$ over all $\nu \in \mathbb{Z}$ using the property $y_{\langle\nu\rangle_N}^{(i)} = y_\nu^{(i)}$. We can relate $s_k^{(i)}$ to $y_\nu^{(i)}$ using the system equations (2.7), (2.8) & (2.9) and the sampled transmission functions defined in Section 2.1

$$\begin{aligned} y_\nu^{(i)} &= \frac{1}{\sqrt{N}} \sum_{n=0}^{N-1} \left( \sum_{m=0}^{N_h-1} h_{t,l}^{(i)}(n, m) \frac{1}{\sqrt{N}} \sum_{k=0}^{N-1} s_k^{(i)} e^{j\frac{2\pi(n-m)}{N}k} + \tilde{w}_n^{(i)} \right) e^{-j\frac{2\pi\nu}{N}n} \\ &= \frac{1}{\sqrt{N}} \sum_{n=0}^{N-1} \tilde{w}_n^{(i)} e^{-j\frac{2\pi\nu}{N}n} \\ &\quad + \sum_{k=0}^{N-1} \left( \frac{1}{\sqrt{N}} \sum_{m=0}^{N_h-1} \left( \frac{1}{\sqrt{N}} \sum_{n=0}^{N-1} h_{t,l}^{(i)}(n, m) e^{-j\frac{2\pi(\nu-k)}{N}n} \right) e^{-j\frac{2\pi k}{N}m} \right) s_k^{(i)} \\ &= w_\nu^{(i)} + \sum_{k=0}^{N-1} \left( \frac{1}{\sqrt{N}} \sum_{m=0}^{N_h-1} h_{d,l}^{(i)}(\nu-k, m) e^{-j\frac{2\pi k}{N}m} \right) s_k^{(i)} \\ &= w_\nu^{(i)} + \sum_{k=0}^{N-1} h_{d,f}^{(i)}(\nu-k, k) s_k^{(i)} \end{aligned} \tag{2.10}$$

Due to the orthonormality of the DFT basis vectors, the frequency-domain noise samples $w_\nu^{(i)}$ are statistically equivalent to their time-domain counterparts namely zero-mean, white and Gaussian with variance $\sigma_w^2$. From (2.10) it is evident that each $y_\nu^{(i)}$ contains contributions from all the $s_k^{(i)}$ transmitted in the $i^{th}$ OFDM block. This phenomenon is known as ICI. The extent of ICI is a function of the rate of channel time-variation within the OFDM block. More explanation about it will be given in Chapter 3. However, even if ICI spans just a few symbols, we clearly see that neglecting it could severely affect the performance of symbol detection. Hence this ICI needs to be explicitly addressed.

If the channel is LTI, ICI is absent (See Appendix A) and thus each $s_k^{(i)}$ can be obtained by simply scaling the corresponding $y_\nu^{(i)}$ followed by thresholding. This simple detection is the original motivation for using cyclic-prefix OFDM in frequency-selective fading channels.

Equation (2.10) can be written in vector form as

$$\underbrace{\begin{bmatrix} y_0^{(i)} \\ y_1^{(i)} \\ \vdots \\ y_{N-1}^{(i)} \end{bmatrix}}_{\mathbf{y}^{(i)}} = \underbrace{\begin{bmatrix} h_{d,f}^{(i)}(0,0) & h_{d,f}^{(i)}(-1,1) & \dots & h_{d,f}^{(i)}(1-N,N-1) \\ h_{d,f}^{(i)}(1,0) & h_{d,f}^{(i)}(0,1) & \dots & h_{d,f}^{(i)}(2-N,N-1) \\ \vdots & \vdots & \ddots & \vdots \\ h_{d,f}^{(i)}(N-1,0) & h_{d,f}^{(i)}(N-2,1) & \dots & h_{d,f}^{(i)}(0,N-1) \end{bmatrix}}_{\mathcal{H}_{d,f}^{(i)}} \underbrace{\begin{bmatrix} s_0^{(i)} \\ s_1^{(i)} \\ \vdots \\ s_{N-1}^{(i)} \end{bmatrix}}_{\mathbf{s}^{(i)}} + \underbrace{\begin{bmatrix} w_0^{(i)} \\ w_1^{(i)} \\ \vdots \\ w_{N-1}^{(i)} \end{bmatrix}}_{\mathbf{w}^{(i)}} \tag{2.11}$$

From a detection standpoint, (2.11) clearly suggests that the basic zero forcing (ZF) detector or the linear minimum mean square error (LMMSE) detector will require a matrix inversion of the Doppler-frequency channel transfer function matrix $\mathcal{H}_{d,f}^{(i)}$. Clearly $\mathcal{H}_{d,f}^{(i)}$ is a non-diagonal $N \times N$ matrix and inverting such a matrix has $\mathcal{O}(N^3)$ complexity.

Modern communication systems employing OFDM prefer large block lengths motivated by the desire to reduce capacity loss due to insertion of redundant guard interval and to maintain narrow subcarrier spacing (to ensure flat fading per carrier) as the system bandwidth increases. This means that the basic ZF and LMMSE detectors will have prohibitive complexity and a new approach needs to be adopted to ensure implementable symbol detection for OFDM in doubly-selective channels.

Since detection strategies often rely on knowledge of the channel coefficients, computationally-efficient channel estimation algorithms are also essential. Presence of significant time-variation increases both the number of channel parameters that must be estimated as well as the difficulty of estimating these parameters.

Thus, clearly, OFDM in doubly-selective environments poses new challenges from an implementation standpoint.

## 2.3 Existing Strategies for OFDM in Doubly-Selective Channels

With very few exceptions, the OFDM literature assumes channels that are constant over the block interval, corresponding to the case in which the subcarriers maintain orthogonality and ICI is avoided. Though intra-block channel-variation is known to degrade performance when ignored (e.g., [13–16]) only a few techniques have been proposed to cope with it. Moreover, none of these techniques appear to be practical from a implementation standpoint.

For example, ICI-mitigating methods have been proposed for flat-fading [17, 18], whereas, OFDM's primary advantage concerns frequency-selective channels. Russell and Stuber [19] have proposed error-control coding and antenna diversity to improve performance. However, these techniques are intended to combat unstructured noise

rather than structured ICI, and hence should be used in addition to explicit ICI reduction. Armstrong et al. [20] have suggested polynomial cancellation coding (PCC) [21] to suppress Doppler-induced ICI based on the fact that PCC is known to suppress ICI resulting from carrier frequency offset. Carrier-offset-induced ICI, however, has a special structure not shared by Doppler-induced ICI, making PCC ineffective. In fact, [20] demonstrated advantages only with fades so flat and slow as to be approximated by a fixed delay. Jeon et al. [22] attacked the problem of intra-block channel variation assuming that the large-variance taps in $\mathcal{H}_{d,f}$ occur primarily along the main diagonal. In Chapter 3 we will show that his assumption was far from accurate.

Linnartz and Gorokhov [23] used a two-term Taylor series expansion to linearly approximate time-domain channel variations and from this designed a MMSE detector. Choi et al. [24], proposed a more general model for the time-variation and derived matched-filter, LS and MMSE detectors that incorporate decision-feedback principles. Though [23,24] are interesting and well formulated, they require the inversion of matrices with dimension equal to the OFDM block length $N$ which is infeasible for large block lengths.

In [25], Giannakis et al. derived a matched filter bound (MFB) for OFDM in doubly-selective fading channels, and showed that channel variations introduce temporal diversity, which has the potential to improve the bit error rate (BER) performance if properly exploited. They also studied the ICI and energy leakage that are caused by the time-varying channel. Next, based on the fact that, ICI power is significant over nearby subcarriers they developed $\mathcal{O}(N^2)$ complexity MMSE and DFE receivers. While the MMSE receiver exhibits an error floor, the DFE receiver does exploit the temporal diversity offered by the channel, and its BER performance comes

close to the MFB for slow-fading channels. Even then, for large block length their algorithms would be impractical to implement.

While channel estimation has been extensively treated in slowly-fading multicarrier systems (with no intra-block channel variation) very little has been proposed for doubly-selective channels. Jeon et al. [22] proposed a simple technique whereby a time-domain Kronecker delta pilot sequence is inserted every $L$ OFDM blocks for easy estimation, and the channel is assumed to change linearly over the $L$ blocks. Clearly this works only for very slowly varying channels. Recently Choi et al. [24] proposed MMSE linear prediction of the LTV impulse response using periodic pilot frames. Specifically, $LN$ pilot observations, collected over a period of $KLN$ samples, are linearly processed to yield joint estimates of $NK$ values of $h_{t,l}(n,m)$, with $n$ centered in the observation period. Requiring $KLN^2$ multiplies and a long processing delay, this is not practical for large $N$.

## 2.4 Our Proposal

Our claim is that the practical application of multicarrier modulation in doubly-selective environments requires a fundamentally new approach to system design and analysis. Traditional cyclic-prefix OFDM has been designed explicitly for the case of non-time-selective fading, and no practical methods have been proposed to handle the challenging combination of time-selectivity and large block length that is expected in future broadband wireless applications. If we accept the fact that interference in the form of ICI and/or ISI is an unavoidable consequence of bandwidth-efficient communication over doubly-selective channels, then we should design multicarrier systems capable of handling this interference in an efficient manner. While ICI increases the

complexity of the standard ZF and LMMSE detectors, it also affords diversity which can be leveraged to increase performance in fading channels. Intuitively speaking, the off-diagonal elements of $\mathcal{H}_{d,f}$ may provide important information about the unknown symbols, when the main diagonal contains small values.

In this thesis, we outline a set of signal processing strategies that constitute a new framework for communication over significantly doubly-selective channels. We focus on practically implementable solutions that offer good performance. A more thorough description of the proposed work will be given in Chapter 4 and Chapter 5. In Chapter 4 we suggest low-complexity linear pre-processing which truncates the ICI response yielding a sparse $\mathcal{H}_{d,f}^{(i)}$ and in Chapter 5 we propose computationally-efficient suboptimal decision-feedback estimation schemes (exploiting the sparse structure of $\mathcal{H}_{d,f}^{(i)}$) which offer good performance relative to the standard detectors but with significant computational savings.

# CHAPTER 3

# THE EFFECT OF A DOUBLY-SELECTIVE FADING CHANNEL ON OFDM

In Chapter 1 we stressed the fact that future wireless applications will face channels that are fairly time- and frequency selective. In Section 2.2 we showed how OFDM in time-selective channels falls prey to ICI. This chapter attempts to quantify this Doppler induced ICI as a function of various system parameters namely, $(i)$ the normalized Doppler frequency, $(ii)$ the variances of the $m^{th}$ lag channel coefficients and $(iii)$ the OFDM block length $N$. In Section 3.1 we describe the basic time-lag channel model that we use in our analysis and simulations. In Section 3.2 we derive the $2^{nd}$ order statistics for the non-sampled Doppler-lag channel taps $H_{d,l}^{(i)}(\phi, m]$. Finally in Section 3.3 we use the results from Section 3.2 to derive the $2^{nd}$ order statistics for the sampled Doppler-frequency channel taps $h_{d,f}^{(i)}(\nu, k)$. From (2.11), we know that $h_{d,f}^{(i)}(\nu, k)$ is the element in the $k^{th}$ column and $\nu^{th}$ diagonal ($\nu = 0$ denotes the main diagonal) of the Doppler-frequency channel transfer function matrix $\mathcal{H}_{d,f}^{(i)}$. Thus the results from Section 3.3 will help us better understand the general structure of $\mathcal{H}_{d,f}$ which is an indicator of the extent of ICI in the OFDM system.

## 3.1 Time-Lag Channel Statistics

We assume a wide-sense stationary uncorrelated scattering (WSSUS) channel where the time-lag channel coefficients $h_{t,l}^{(i)}(n,m)$ are correlated over time-$n$ and are independent over lag-$m$ so that,

$$\mathrm{E}\{h_{t,l}^{(i)}(n,m)h_{t,l}^{(i)^*}(n-p,m-l)\} = \begin{cases} 0 & l \neq 0 \\ \sigma_m^2 J_0(2\pi f_d p) & l = 0 \end{cases} \tag{3.1}$$

where $J_0(\cdot)$ is zero-order Bessel function of first kind, and $f_d$ is the (maximum) normalized Doppler frequency[4] defined by

$$f_d = \frac{f_c\, v\, T_s}{c}$$

where $f_c$ is the carrier frequency, $v$ the mobile velocity, $T_s$ the sampling interval and $c$ the speed of light. Henceforth we define the autocorrelation for the $m^{th}$ lag as

$$r_{t,l}(p,m) = \mathrm{E}\{h_{t,l}^{(i)}(n,m)h_{t,l}^{(i)^*}(n-p,m)\}$$

As mentioned in Section 2.2 the channel is assumed to change continuously over $n$ as well as over $i$.

## 3.2 Doppler-Lag Channel Statistics

From (2.3) we know that the non-sampled Doppler-lag response is given by

$$H_{d,l}(\phi,m) = \frac{1}{\sqrt{N}} \sum_{n=0}^{N-1} h_{t,l}(n,m)e^{-j\phi n}$$

where the limits on $n$ are due to the finite OFDM block length $N$. We have

$$\begin{aligned} &\mathrm{E}\{H_{d,l}^{(i)}(\phi,m)H_{d,l}^{(i)^*}(\phi-\Delta,m)\} \\ &\quad = \mathrm{E}\left\{ \frac{1}{\sqrt{N}} \sum_{n=0}^{N-1} h_{t,l}^{(i)}(n,m)e^{-j\phi n} \frac{1}{\sqrt{N}} \sum_{l=0}^{N-1} h_{t,l}^{(i)^*}(l,m)e^{j(\phi-\Delta)l} \right\} \end{aligned}$$

[4] Observe $f_d$ is unitless.

$$
\begin{aligned}
&= \frac{1}{N}\sum_{n=0}^{N-1}\sum_{l=0}^{N-1} \mathrm{E}\{h_{t,l}^{(i)}(n,m)h_{t,l}^{(i)^*}(l,m)\}e^{-j\phi n}e^{j(\phi-\Delta)l} \\
&= \frac{1}{N}\sum_{n=0}^{N-1}\sum_{l=0}^{N-1} r_{t,l}(n-l,m)e^{-j\phi(n-l)}e^{-j\Delta l} \qquad (3.2)\\
&= \frac{1}{N}\sum_{p=0}^{N-1}\sum_{l=0}^{N-1-p} r_{t,l}(p,m)e^{-j\phi p}e^{-j\Delta l} + \frac{1}{N}\sum_{p=-1}^{-N+1}\sum_{l=-p}^{N-1} r_{t,l}(p,m)e^{-j\phi p}e^{-j\Delta l} \\
&= \frac{1}{N}\sum_{p=0}^{N-1} r_{t,l}(p,m)e^{-j\phi p}\sum_{l=0}^{N-1-p} e^{-j\Delta l} + \frac{1}{N}\sum_{p=-1}^{-N+1} r_{t,l}(p,m)e^{-j(\phi-\Delta)p}\sum_{l=0}^{N-1+p} e^{-j\Delta l}
\end{aligned}
$$

Using the Dirichlet sinc function

$$
\sum_{l=0}^{L-1} e^{-j\Delta l} = \frac{\sin(\Delta L/2)}{\sin(\Delta/2)}e^{-j\frac{\Delta}{2}(L-1)} \qquad (3.3)
$$

we have

$$
\begin{aligned}
&\mathrm{E}\{H_{d,l}^{(i)}(\phi,m)H_{d,l}^{(i)^*}(\phi-\Delta,m)\} \\
&\quad= \frac{1}{N}\sum_{p=0}^{N-1} r_{t,l}(p,m)e^{-j\phi p}\frac{\sin(\Delta(N-p)/2)}{\sin(\Delta/2)}e^{-j\frac{\Delta}{2}(N-p-1)} \\
&\qquad + \frac{1}{N}\sum_{p=-1}^{-N+1} r_{t,l}(p,m)e^{-j(\phi-\Delta)p}\frac{\sin(\Delta(N+p)/2)}{\sin(\Delta/2)}e^{-j\frac{\Delta}{2}(N+p-1)} \\
&\quad= \frac{1}{N}\sum_{p=0}^{N-1} r_{t,l}(p,m)e^{-j(\phi-\frac{\Delta}{2})p}\frac{\sin(\Delta(N-p)/2)}{\sin(\Delta/2)}e^{-j\frac{\Delta}{2}(N-1)} \\
&\qquad + \sum_{p=-1}^{-N+1} r_{t,l}(p,m)e^{-j(\phi-\frac{\Delta}{2})p}\frac{\sin(\Delta(N+p)/2)}{\sin(\Delta/2)}e^{-j\frac{\Delta}{2}(N-1)} \\
&\quad= \frac{1}{N}\sum_{p=-N+1}^{N-1} r_{t,l}(p,m)e^{-j(\phi-\frac{\Delta}{2})p}\frac{\sin(\Delta(N-|p|)/2)}{\sin(\Delta/2)}e^{-j\frac{\Delta}{2}(N-1)}
\end{aligned}
$$

We can interpret the previous expression using a $\Delta$-parameterized lag-domain window

$$
w(\Delta,m) = \frac{\sin(\Delta(N-|p|)/2)}{\sin(\Delta/2)}e^{-j\frac{\Delta}{2}(N-p-1)}I_{[0,N-1]}(|p|)
$$

via the indicator function

$$I_{[0,N-1]}(|p|) = \begin{cases} 1 & |p| \in [0, N-1] \\ 0 & \text{else} \end{cases}$$

so that

$$\mathrm{E}\{H_{d,l}^{(i)}(\phi, m) H_{d,l}^{(i)^*}(\phi - \Delta, m)\} = \sum_{p=-\infty}^{\infty} r_{t,l}(p, m) w(\Delta, p) e^{-j\phi p} \tag{3.4}$$

Two interesting properties of the window function are

$$\begin{aligned} w(\Delta, p)|_{\Delta=0} &= \left(\frac{N - |p|}{N}\right) I_{[0,N-1]}(|p|) \\ \lim_{N\to\infty} w(\Delta, p) &= \begin{cases} 1 & \Delta = 0 \\ 0 & \Delta \neq 0 \end{cases} \quad \forall p \in \mathbb{Z} \end{aligned}$$

implying that

$$\lim_{N\to\infty} \mathrm{E}\{H_{d,l}^{(i)}(\phi, m) H_{d,l}^{(i)^*}(\phi - \Delta, m)\} = \begin{cases} S_{d,l}(\phi, m) & \Delta = 0 \\ 0 & \Delta \neq 0 \end{cases}$$

where $S_{d,l}(\phi, m)$ denotes the Doppler spectrum of the lag-$m$ channel coefficient:

$$\begin{aligned} S_{d,l}(\phi, m) &= \sum_{p=-\infty}^{\infty} r_{t,l}(p, m) e^{-j\phi p} \\ &= \begin{cases} \frac{\sigma_m^2}{\sqrt{(2\pi f_d)^2 - \phi^2}} & |\phi| \leq 2\pi f_d \\ 0 & \text{else} \end{cases} \end{aligned}$$

The window function can be expressed in the frequency domain as

$$\begin{aligned} W(\Delta, \phi) &= \sum_{p=-\infty}^{\infty} w(\Delta, p) e^{-j\phi p} \\ &= \mathrm{E}\{H_{d,l}^{(i)}(\phi, m) H_{d,l}^{(i)^*}(\phi - \Delta, m)\}\Big|_{r_{t,l}(p,m)=1 \ \ \forall p} \\ &= \frac{1}{N} \sum_{n=0}^{N-1} e^{-j\phi n} \sum_{l=0}^{N-1} e^{j(\phi - \Delta)l} \qquad (3.5) \\ &= \frac{1}{N} \frac{\sin(\phi N/2)}{\sin(\phi/2)} e^{-j\frac{\phi}{2}(N-1)} \frac{\sin((\phi - \Delta)N/2)}{\sin((\phi - \Delta)/2)} e^{j\frac{(\phi-\Delta)}{2}(N-1)} \qquad (3.6) \\ &= \frac{1}{N} \frac{\sin(\phi N/2)}{\sin(\phi/2)} \frac{\sin((\phi - \Delta)N/2)}{\sin((\phi - \Delta)/2)} e^{-j\frac{\Delta}{2}(N-1)} \end{aligned}$$

where (3.5) and (3.6) follow from (3.2) and (3.3) respectively. Some properties of the frequency-domain version of the window function are

$$\begin{aligned} W(\Delta,\phi)|_{\Delta=0} &= \frac{1}{N}\left(\frac{\sin(\phi N/2)}{\sin(\phi/2)}\right)^2 \\ \lim_{N\to\infty}\frac{1}{N}W(\Delta,\phi) &= \begin{cases} 1 & \Delta=\phi=0 \\ 0 & \text{else} \end{cases} \end{aligned}$$

This frequency-domain description is useful in that (3.4) can be rewritten as

$$\begin{aligned} \mathrm{E}\{H_{d,l}^{(i)}(\phi,m)H_{d,l}^{(i)^*}(\phi-\Delta,m)\} &= \int_{-\pi}^{\pi} S_{d,l}(\theta,m)W(\Delta,\phi-\theta)d\theta \\ &= S_{d,l}(\phi,m) * W(\Delta,\phi) \end{aligned}$$

where "$*$" denotes convolution as defined above. Finally, we note that

$$\mathrm{E}\{H_{d,l}^{(i)}(\phi,m)H_{d,l}^{(i)^*}(\phi-\Delta,m-\rho)\}=0, \quad \forall\rho\neq 0$$

## 3.3 Doppler-Frequency Channel Statistics

From (2.5) we know that the non-sampled Doppler-frequency response is denoted by

$$\begin{aligned} H_{d,f}(\phi,\omega) &= \frac{1}{\sqrt{N}}\sum_{m=0}^{N_h-1} H_{d,l}(\phi,m)e^{-j\omega m} \\ &= \frac{1}{\sqrt{N}}\sum_{m=0}^{N-1} H_{d,l}(\phi,m)e^{-j\omega m} \end{aligned}$$

we have

$$\begin{aligned} &\mathrm{E}\{H_{d,f}^{(i)}(\phi,\omega)H_{d,f}^{(i)^*}(\phi-\Delta,\omega-\psi)\} \\ &\quad= \mathrm{E}\left\{\frac{1}{\sqrt{N}}\sum_{m=0}^{N-1} H_{d,l}^{(i)}(\phi,m)e^{-j\omega m}\frac{1}{\sqrt{N}}\sum_{q=0}^{N-1} H_{d,l}^{(i)^*}(\phi-\Delta,q)e^{j(\omega-\psi)q}\right\} \\ &\quad= \frac{1}{N}\sum_{m=0}^{N-1}\sum_{q=0}^{N-1}\mathrm{E}\{H_{d,l}^{(i)}(\phi,m)H_{d,l}^{(i)^*}(\phi-\Delta,q)\}e^{-j\omega m}e^{j(\omega-\psi)q} \end{aligned}$$

$$
\begin{aligned}
&= \frac{1}{N}\sum_{m=0}^{N-1} \mathrm{E}\{H_{d,l}^{(i)}(\phi,m)H_{d,l}^{(i)^*}(\phi-\Delta,m)\}e^{-j\psi m} \\
&= \left(\sum_{m=0}^{N-1} S_{d,l}(\phi,m)e^{-j\psi m}\right) * \frac{1}{N}W(\Delta,\phi) \\
&= S_{d,f}(\phi,\psi) * \frac{1}{N}W(\Delta,\phi)
\end{aligned}
$$

where $S_{d,f}(\phi,\psi)$ denotes the Doppler-frequency spectrum:

$$
S_{d,f}(\phi,\psi) = \begin{cases} \frac{\sum_{m=0}^{N_h-1}\sigma_m^2 e^{-j\psi m}}{\sqrt{(2\pi f_d)^2-\phi^2}} & |\phi| \le 2\pi f_d \\ 0 & \text{else} \end{cases}
$$

The sampled Doppler-frequency statistics are then

$$
\mathrm{E}\{h_{d,f}^{(i)}(\nu,k)h_{d,f}^{(i)^*}(\nu-\rho,k-l)\} = \frac{1}{N}S_{d,f}\left(\phi,\frac{2\pi l}{N}\right) * W\left(\phi,\frac{2\pi\rho}{N}\right)\Big|_{\phi=\frac{2\pi\nu}{N}}
$$

Hence the variance equals

$$
\mathrm{E}\{|h_{d,f}^{(i)}(\nu,k)|^2\} = \left(\frac{\sum_{m=0}^{N_h-1}\sigma_m^2}{\sqrt{(2\pi f_d)^2-\phi^2}} I_{[0,2\pi f_d)}(|\phi|)\right) * \left(\frac{\sin(\phi N/2)}{N\sin(\phi/2)}\right)^2\Bigg|_{\phi=\frac{2\pi\nu}{N}} \tag{3.7}
$$

As mentioned before, $h_{d,f}(\nu,k)$ represents the element in the $k^{th}$ column and $\nu^{th}$ diagonal ($\langle\nu\rangle_N = \nu$) of $\mathcal{H}_{d,f}$. Equation (3.7) suggests that $|h_{d,f}(\nu,k)|$ will have reasonably large values for small values of $\nu$, which correspond to the terms that significantly contribute towards the system ICI power. On the other hand $|h_{d,f}(\nu,k)|$ will have relatively small values for large values of $\nu$, which correspond to the terms that have a very small contribution towards the system ICI power.

Clearly the extent of ICI is proportional to the fading rate (characterized by $f_d$) exhibited by the channel. For channels that do not exhibit time-selectivity ($f_d = 0$), $|h_{d,f}(\nu,k)| = 0$ for $\nu \neq 0$. In Fig. 3.1 we evaluate (3.7) for block length $N = 64$, unit variance lag coefficients and various $f_d$.

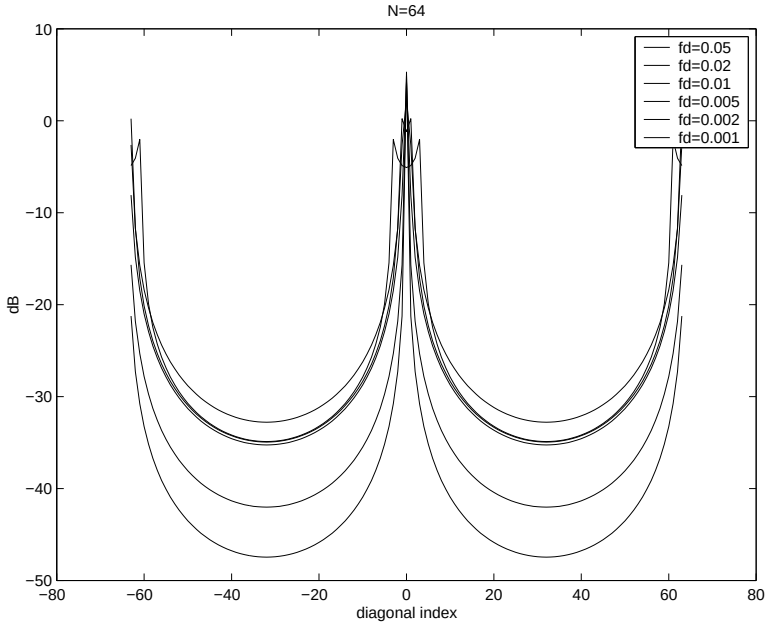


Figure 3.1: Variance of elements in $\mathcal{H}_{d,f}$ vs. Doppler spread

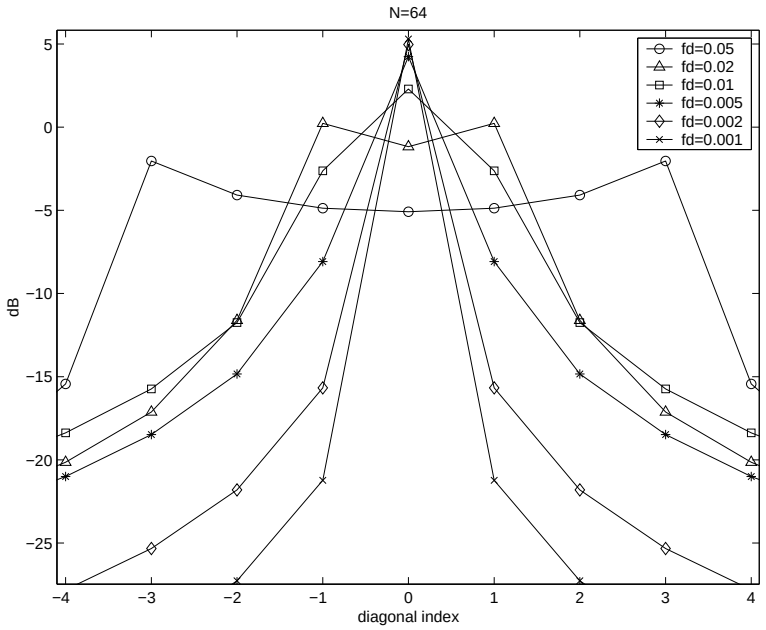


Figure 3.2: A close up of Fig. 3.1

Observe that even relatively slow channels: channels for which the Doppler spread is much less than the intercarrier spacing (i.e., $f_d \ll 1/N$) exhibit significant ICI power.

# CHAPTER 4

# DOPPLER-CHANNEL SHORTENING VIA LINEAR RECEIVER PROCESSING

## 4.1 Motivation

The OFDM receiver observes the output of the noisy linear channel and discards the samples corresponding to the prefix, after which the time-domain observation sequence for the $i^{th}$ OFDM block can be written in vector form as (See (2.8))

$$\mathbf{r}^{(i)} = \mathcal{H}_{t,l}^{(i)} \mathbf{F}^H \mathbf{s}^{(i)} + \tilde{\mathbf{w}}^{(i)} \tag{4.1}$$

In (4.1), $\mathbf{s}^{(i)}$ denotes a vector of frequency-domain QAM symbols transmitted in the $i^{th}$ OFDM block, $\mathbf{F}^H$ a unitary matrix representing the inverse $N$-FFT operation defined elementwise as

$$[\mathbf{F}^H]_{i,k} = \frac{1}{\sqrt{N}} e^{j\frac{2\pi}{N}ik},$$

$\mathcal{H}_{t,l}^{(i)}$ is the time-lag channel transfer function matrix representing the time-domain effect of the channel and $\tilde{\mathbf{w}}^{(i)}$ a vector of zero-mean white and Gaussian noise samples with variance $\sigma_w^2$. Performing an $N$-point FFT at the receiver (denoted by $\mathbf{F}$), we

obtain the frequency-domain observation vector (See (2.9))

$$\begin{aligned} \mathbf{y}^{(i)} &= \mathbf{F}\mathbf{r}^{(i)} \\ &= \mathbf{F}\mathcal{H}_{t,l}^{(i)}\mathbf{F}^H\mathbf{s}^{(i)} + \mathbf{F}\tilde{\mathbf{w}}^{(i)} \\ &= \mathcal{H}_{d,f}^{(i)}\mathbf{s}^{(i)} + \mathbf{w}^{(i)} \end{aligned} \tag{4.2}$$

where $\mathcal{H}_{d,f}^{(i)}$ is the Doppler-frequency transfer function matrix that represents the frequency-domain effect of the channel and $\mathbf{w}^{(i)}$ is a vector containing frequency-domain noise samples.

For LTI channels (no Doppler spread), $\mathcal{H}_{t,l}$ is a circulant matrix and $\mathcal{H}_{d,f}$ is diagonal. Here, optimal detection of the $k^{th}$ element in $\mathbf{s}$ can be accomplished using only the $k^{th}$ element of $\mathbf{y}$ and the $k^{th}$ diagonal element of $\mathcal{H}_{d,f}$. When the Doppler spread is non-trivial (LTV channels), $\mathcal{H}_{t,l}$ loses its circulant structure, preventing $\mathcal{H}_{d,f}$ from being diagonal (See (2.11)) which causes ICI and complicates the detection of $\mathbf{s}$. While standard detection strategies (e.g., ZF, LMMSE and MLSD [26]) are easy to formulate, they are impractical to implement when the dimension of $\mathcal{H}_{d,f}$ (given by the OFDM block length, which may be $> 8000$) is large. In Chapter 3 we derived an expression for the variance of the elements in $\mathcal{H}_{d,f}$ which suggests that, on average, the magnitudes of the off-diagonal elements decay slowly with increasing distance from the main-diagonal (See Fig. 3.2), i.e., ICI is worst among "nearby" subcarriers. Thus, incorporating the effects of distant-ICI might improve the detection performance but prevents practical implementation.

In this chapter, we propose low-complexity linear receiver pre-processing to truncate the off-diagonal (i.e., ICI) response of $\mathcal{H}_{d,f}$. While $\mathcal{H}_{d,f}$ could obviously be diagonalized through the "zero-forcing" linear transformation $\mathcal{H}_{d,f}^{-1}$, this has two major

disadvantages: $(i)$ the $\mathcal{O}(N^3)$ complexity of matrix inversion, and $(ii)$ the potential for noise gain: $\mathcal{H}_{d,f}^{-1}\mathbf{y} = \mathbf{s} + \mathcal{H}_{d,f}^{-1}\mathbf{w}$ where $\mathcal{H}_{d,f}^{-1}\mathbf{w}$ may be large. Instead, we propose to "shorten the ICI response", resulting in so-called "controlled ICI" that can be efficiently handled with appropriate detection algorithms (discussed in Chapter 5). This is analogous to ISI-channel shortening employed in single-carrier systems to reduce the complexity of maximum likelihood sequence detection (MLSD) [12, 27].

While single-carrier systems typically accomplish ISI-shortening using convolutive filtering, we propose ICI-shortening using "fast convolution" [28] in order to leverage the FFT operation already being performed by the OFDM receiver. The simplest approach would involve "windowing" the $N$-point time-domain received signal $\mathbf{r}^{(i)}$ prior to the FFT. Windowing has been proposed as a computationally-efficient means of increasing the decay rate of the resulting ICI terms (e.g., [29–33]). In those papers, the time-domain transmitted and/or received signals were multiplied by a sequence of window coefficients typically chosen from the well-known Hann, Kaiser, or Blackman shapes [34]. While these particular windows have been shown to reduce ICI, they are not optimal for this application, leaving room for significant improvement.

In this chapter we propose the design of statistically-optimal windows based on appropriate statistical fading models [35]. While it would be possible to design these windows to minimize the variance of all ICI, this may be foolish from a "diversity" standpoint: In the event that the diagonal elements were very small (i.e. faded), off-diagonal elements may contain critical information for symbol detection. For this reason, we propose windows which allow controlled ICI and where the "target ICI" is optimized jointly with the window.

Ideally, the ICI-shortening window should be optimized to maximize symbol detection performance. If we assume an OFDM system employing powerful error-control coding, then the final detection performance is proportional to the average signal to interference-plus-noise ratio (SINR) across carriers [36], and "SINR optimization" becomes the optimal criterion. Here, interference refers to the contributions from the non-controlled ICI.

In fact, one could take the windowing concept further: recall, that $\mathbf{r}^{(i)}$ has been rectangularly windowed in the guard removal step to prevent inter-block interference (IBI). Given that multipath channels typically exhibit an exponentially decaying delay profile [35], it is likely that a small amount of IBI can be traded for a larger reduction in ICI. Thus, an improved strategy would involve windowing an $N + N_p + N_h$-point segment of the received signal, where $N_p$ denotes the cyclic prefix length and $N_h$ the maximum channel delay spread in baud. In addition, viewing these windowing operations as diagonal matrix multiplications, a banded matrix multiplication, or "super-windowing" may offer yet improved performance at a relatively small complexity increase.

In this thesis, we focus on the basic $N$-point window designed to maximize SINR. Section 4.2 explains the effect of time-domain windowing on OFDM and provides the set up required for the optimal-window design. In Section 4.3 we derive an expression for the coefficients of the window that maximizes the SINR in terms of the channel response $h_{t,l}(n, m)$, AWGN variance $\sigma_w^2$ and the desired ICI-spread $D$. Finally, for channels with significant delay spread, we can show that the SINR-optimal window is well approximated by a function of only channel and noise statistics (i.e.,

not realizations), which is very advantageous from an implementation standpoint. Specifics are provided in Section 4.4.

## 4.2 Effect of Time-Domain Windowing

A "windowing" receiver applies a time-domain window with coefficients $b(n)$ before taking the DFT, yielding the output $\{\overline{y}_\nu^{(i)}\}_{\nu=0}^{N-1}$

$$\overline{y}_\nu^{(i)} = \frac{1}{\sqrt{N}} \sum_{n=0}^{N-1} b(n)\, r^{(i)}(n) e^{-j\frac{2\pi\nu}{N}n} \tag{4.3}$$

These windowed frequency-domain received samples can be related to their non-windowed counterparts from (2.9) as

$$\overline{y}_\nu^{(i)} = \frac{1}{\sqrt{N}} \sum_{n=0}^{N-1} \sum_{l=0}^{N-1} b(l)\, r^{(i)}(n) \delta_{n-l} e^{-j\frac{2\pi\nu}{N}n}$$

where $\delta_k$ is a Dirac-delta function function defined as

$$\delta_k = \begin{cases} 1 & k = 0 \\ 0 & \text{else} \end{cases}$$

So,

$$\begin{aligned} \overline{y}_\nu^{(i)} &= \frac{1}{\sqrt{N}} \sum_{n=0}^{N-1} \sum_{l=0}^{N-1} b(l)\, r^{(i)}(n) \left( \frac{1}{N} \sum_{p=0}^{N-1} e^{-j\frac{2\pi(l-n)}{N}p} \right) e^{-j\frac{2\pi\nu}{N}n} \\ &= \frac{1}{\sqrt{N}} \sum_{p=0}^{N-1} \left( \frac{1}{\sqrt{N}} \sum_{l=0}^{N-1} b(l) e^{-j\frac{2\pi p}{N}l} \right) \left( \frac{1}{\sqrt{N}} \sum_{n=0}^{N-1} r^{(i)}(n) e^{-j\frac{2\pi(\nu-p)}{N}n} \right) \\ &= \frac{1}{\sqrt{N}} \sum_{p=0}^{N-1} B_p y_{\nu-p}^{(i)} \end{aligned} \tag{4.4}$$

This can be derived using the $N \times N$ DFT matrix $\mathbf{F}$, defined elementwise as

$$[\mathbf{F}]_{i,k} = \frac{1}{\sqrt{N}} e^{-j\frac{2\pi}{N}ik},$$

the vector-to-diagonal matrix operator $\mathcal{D}(\cdot)$, the vector-to-circulant matrix operator $\mathcal{C}(\cdot)$, and the DFT property [37]

$$\mathbf{F}\mathcal{D}(\mathbf{b})\mathbf{F}^H = \frac{1}{\sqrt{N}}\mathcal{C}(\underbrace{\mathbf{F}\mathbf{b}}_{\mathbf{B}}) \tag{4.5}$$

as follows

$$\begin{aligned}
\overline{\mathbf{y}}^{(i)} &= \mathbf{F}\mathcal{D}(\mathbf{b})\mathbf{r}^{(i)} \\
&= \mathbf{F}\mathcal{D}(\mathbf{b})\mathbf{F}^H\mathbf{F}\mathbf{r}^{(i)} \\
&= \frac{1}{\sqrt{N}}\mathcal{C}(\mathbf{B})\mathbf{y}^{(i)} \\
&= \frac{1}{\sqrt{N}}\mathcal{C}(\mathbf{B})\left(\mathcal{H}_{d,f}^{(i)}\mathbf{s}^{(i)} + \mathbf{w}^{(i)}\right)
\end{aligned} \tag{4.6}$$

The aim of windowing is to make the matrix $\mathcal{C}(\mathbf{B})\mathcal{H}_{d,f}^{(i)}$ sparse, which reduces the number of significant channel coefficients to be handled by the receiver, thereby reducing the complexity of the symbol detection.

In fact, as detection concerns, the receiver assumes that the windowed channel matrix $\mathcal{C}\left(\mathbf{B}\right)\mathcal{H}_{d,f}^{(i)}$ has many zero-valued elements, and any elements wrongfully assumed to be zero will contribute to the overall level of interference. The interference level can be quantified with the aid of a mask operator $\mathcal{M}(\cdot)$ which nulls any matrix elements assumed zero by the receiver and the complementary masking operator $\overline{\mathcal{M}}(\cdot)$ which nulls the elements assumed non-zero by the receiver. The effective "signal" and "noise + interference" components are then

$$\begin{aligned}
\text{"signal"} &= \frac{1}{\sqrt{N}}\mathcal{M}\left(\mathcal{C}\left(\mathbf{B}\right)\mathcal{H}_{d,f}^{(i)}\right)\mathbf{s}^{(i)} \\
\text{"noise + interference"} &= \frac{1}{\sqrt{N}}\overline{\mathcal{M}}\left(\mathcal{C}\left(\mathbf{B}\right)\mathcal{H}_{d,f}^{(i)}\right)\mathbf{s}^{(i)} + \frac{1}{\sqrt{N}}\mathcal{C}\left(\mathbf{B}\right)\mathbf{w}^{(i)}
\end{aligned}$$

yielding the following "signal" and "noise+interference" energies (assuming $\mathrm{E}\{\mathbf{s}^{(i)}\mathbf{s}^{(i)H}\} = \mathbf{I}$, $\mathrm{E}\{\mathbf{w}^{(i)}\mathbf{w}^{(i)H}\} = \sigma_w^2\mathbf{I}$ and $\mathrm{E}\{\mathbf{s}^{(i)}\mathbf{w}^{(i)H}\} = \mathbf{0}$)

$$\begin{aligned}\mathcal{E}_s &= \frac{1}{N}\|\mathcal{M}\left(\mathcal{C}\left(\mathbf{B}\right)\mathcal{H}_{d,f}^{(i)}\right)\|_F^2 \\ \mathcal{E}_{ni} &= \frac{1}{N}\|\overline{\mathcal{M}}\left(\mathcal{C}(\mathbf{B})\mathcal{H}_{d,f}^{(i)}\right)\|_F^2 + \frac{\sigma_w^2}{N}\|\mathcal{C}(\mathbf{B})\|_F^2\end{aligned}$$

where $\|\cdot\|$ denotes the Frobenius norm.

## 4.3 Max-SINR Window Design

From equation (3.7) and Fig. 3.1, we are motivated to choose an "adjacent-carrier" desired ICI region, i.e., $\mathcal{C}(\mathbf{B})\mathcal{H}_{d,f}^{(i)}$ with a banded structure (including the top-right and bottom-left corners). Equivalently, the mask operator $\mathcal{M}(\cdot)$ nulls the $\nu^{th}$ diagonal for each $\nu$ in the range $D+1 \leq \langle\nu\rangle_N \leq N-D-1$, where $\nu = 0$ corresponds to the main diagonal. The parameter $D$ controls the target level of ICI shortening:

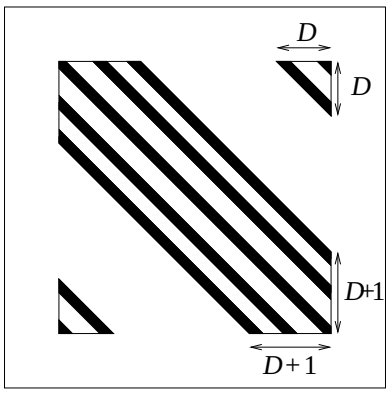


Figure 4.1: Choosing the mask

smaller $D$ corresponds to a shorter ICI span and thus reduced detection complexity.

While technically we require $0 \leq D \leq \frac{N}{2} - 1$, we have observed that, for good window performance, $D$ must be chosen in accordance with the Doppler spread.

Our definition of $\mathcal{M}(\cdot)$ allows the simplification

$$\|\mathcal{M}\left(\mathcal{C}\left(\mathbf{B}\right)\mathcal{H}_{d,f}^{(i)}\right)\|_F^2 = \|\mathcal{P}\mathcal{C}\left(\mathbf{B}\right)\mathbf{H}_{d,f}^{(i)}\|_F^2$$

where

$$\mathcal{P} = \begin{bmatrix} \mathbf{I}_{D+1} & \mathbf{0} & \mathbf{0} \\ \mathbf{0} & \mathbf{0} & \mathbf{0} \\ \mathbf{0} & \mathbf{0} & \mathbf{I}_D \end{bmatrix}$$

and $\mathbf{H}_{d,f}^{(i)}$ is a re-arrangement of $\mathcal{H}_{d,f}^{(i)}$ defined elementwise by

$$[\mathbf{H}_{d,f}^{(i)}]_{\nu,k} = h_{d,f}^{(i)}(\nu, k).$$

Similarly we have

$$\|\overline{\mathcal{M}}\left(\mathcal{C}\left(\mathbf{B}\right)\mathcal{H}_{d,f}^{(i)}\right)\|_F^2 = \|\mathcal{P}^{\perp}\mathcal{C}\left(\mathbf{B}\right)\mathbf{H}_{d,f}^{(i)}\|_F^2$$

where $\mathcal{P}^{\perp} = \mathbf{I}_N - \mathcal{P}$. Noting that

$$\begin{aligned}
\|\mathcal{C}(\mathbf{B})\|_F^2 &= N\|\mathbf{b}\|^2 \\
\|\mathcal{C}(\mathbf{B})\mathbf{H}_{d,f}^{(i)}\|_F^2 &= N\|\mathbf{F}\mathcal{D}(\mathbf{b})\mathbf{F}^H\mathbf{H}_{d,f}^{(i)}\mathbf{F}\|_F^2 \\
&= N\|\mathcal{D}(\mathbf{b})\mathbf{H}_{t,l}^{(i)}\|_F^2 \\
&= N\mathbf{b}^H\mathrm{diag}(\mathbf{H}_{t,l}^{(i)}{\mathbf{H}_{t,l}^{(i)}}^H)\mathbf{b} \\
\|\mathcal{P}\mathcal{C}(\mathbf{B})\mathbf{H}_{d,f}^{(i)}\|_F^2 &= N\|\mathcal{P}\mathbf{F}\mathcal{D}(\mathbf{b})\mathbf{H}_{t,l}^{(i)}\|_F^2
\end{aligned}$$

where

$$[\mathbf{H}_{t,l}^{(i)}]_{n,m} = h_{t,l}^{(i)}(n, m)$$

and that

$$\begin{aligned}\|\mathcal{C}(\mathbf{B})\mathbf{H}_{d,f}^{(i)}\|_F^2 &= \|(\mathcal{P}+\mathcal{P}^{\perp})\mathcal{C}(\mathbf{B})\mathbf{H}_{d,f}^{(i)}\|_F^2 \\ &= \|\mathcal{P}\mathcal{C}(\mathbf{B})\mathbf{H}_{d,f}^{(i)}\|_F^2 + \|\mathcal{P}^{\perp}\mathcal{C}(\mathbf{B})\mathbf{H}_{d,f}^{(i)}\|_F^2\end{aligned}$$

so that

$$\begin{aligned}\|\mathcal{P}^{\perp}\mathcal{C}(\mathbf{B})\mathbf{H}_{d,f}^{(i)}\|_F^2 &= \|\mathcal{C}(\mathbf{B})\mathbf{H}_{d,f}^{(i)}\|_F^2 - \|\mathcal{P}\mathcal{C}(\mathbf{B})\mathbf{H}_{d,f}^{(i)}\|_F^2 \\ &= N\mathbf{b}^H \mathrm{diag}(\mathbf{H}_{t,l}^{(i)}{\mathbf{H}_{t,l}^{(i)}}^H)\mathbf{b} - N\|\mathcal{P}\mathbf{F}\mathcal{D}(\mathbf{b})\mathbf{H}_{t,l}^{(i)}\|_F^2\end{aligned}$$

Maximizing SINR $\mathcal{E}_s/\mathcal{E}_{ni}$ is accomplished by

$$\begin{aligned}\mathbf{b}_\star &= \arg\max_{\mathbf{b}} \frac{\|\mathcal{P}\mathcal{C}(\mathbf{B})\mathbf{H}_{d,f}^{(i)}\|_F^2}{\|\mathcal{P}^{\perp}\mathcal{C}(\mathbf{B})\mathbf{H}_{d,f}^{(i)}\|_F^2 + \sigma_w^2\|\mathcal{C}(\mathbf{B})\|_F^2} \\ &= \arg\max_{\mathbf{b}} \frac{\|\mathcal{P}\mathbf{F}\mathcal{D}(\mathbf{b})\mathbf{H}_{t,l}^{(i)}\|_F^2}{\mathbf{b}^H \mathrm{diag}(\sigma_w^2\mathbf{I} + \mathbf{H}_{t,l}^{(i)}{\mathbf{H}_{t,l}^{(i)}}^H)\mathbf{b} - \|\mathcal{P}\mathbf{F}\mathcal{D}(\mathbf{b})\mathbf{H}_{t,l}^{(i)}\|_F^2}\end{aligned}$$

This can be solved in closed form through

$$\begin{aligned}\tilde{\mathbf{b}} &= \mathrm{diag}(\sigma_w^2\mathbf{I} + \mathbf{H}_{t,l}^{(i)}{\mathbf{H}_{t,l}^{(i)}}^H)^{\frac{1}{2}}\mathbf{b} \\ \tilde{\mathbf{b}}_\star &= \arg\max_{\tilde{\mathbf{b}}} \frac{\|\mathcal{P}\mathbf{F}\mathcal{D}(\tilde{\mathbf{b}})\tilde{\mathbf{H}}_{t,l}^{(i)}\|_F^2}{\|\tilde{\mathbf{b}}\|^2 - \|\mathcal{P}\mathbf{F}\mathcal{D}(\tilde{\mathbf{b}})\tilde{\mathbf{H}}_{t,l}^{(i)}\|_F^2}\end{aligned}$$

using

$$\tilde{\mathbf{H}}_{t,l}^{(i)} = \mathrm{diag}(\sigma_w^2\mathbf{I} + \mathbf{H}_{t,l}^{(i)}{\mathbf{H}_{t,l}^{(i)}}^H)^{-\frac{1}{2}}\mathbf{H}_{t,l}^{(i)} \tag{4.7}$$

Noting that the SINR is invariant to the scaling of $\tilde{\mathbf{b}}$, we can assume without any loss of generality that $\|\tilde{\mathbf{b}}\| = 1$, in which case

$$\tilde{\mathbf{b}}_\star = \arg\max_{\|\tilde{\mathbf{b}}\|=1} \|\mathcal{P}\mathbf{F}\mathcal{D}(\tilde{\mathbf{b}})\tilde{\mathbf{H}}_{t,l}^{(i)}\|_F^2$$

It helps to write the above norm as

$$\begin{aligned}\|\mathcal{P}\mathbf{F}\mathcal{D}(\tilde{\mathbf{b}})\tilde{\mathbf{H}}_{t,l}^{(i)}\|_F^2 &= \sum_{m=0}^{N_h-1}\sum_{|k|\le D}\left|\frac{1}{\sqrt{N}}\sum_{n=0}^{N-1}\tilde{b}_n e^{-j\frac{2\pi k}{N}n}\tilde{h}_{t,l}^{(i)}(n,m)\right|^2 \\ &= \frac{1}{N}\sum_{n,l}\tilde{b}_n\tilde{b}_l^*\sum_{|k|\le D}e^{-j\frac{2\pi(n-l)}{N}k}\sum_{m=0}^{N_h-1}\tilde{h}_{t,l}^{(i)}(n,m)\tilde{h}_{t,l}^{(i)^*}(l,m) \\ &= \tilde{\mathbf{b}}^H\mathbf{A}\tilde{\mathbf{b}}\end{aligned}$$

where $\mathbf{A}$ is defined below (using $\odot$ to denote elementwise multiplication):

$$\mathbf{A} = \frac{1}{N}\sum_{|k|\le D}e^{-j\frac{2\pi(n-l)}{N}k}\cdot\sum_{m=0}^{N_h-1}\tilde{h}_{t,l}^{(i)}(n,m)\tilde{h}_{t,l}^{(i)^*}(l,m) \tag{4.8}$$

$$= \mathbf{A}_1\odot\mathbf{A}_2 \quad \text{for} \quad \begin{cases}[\mathbf{A}_1]_{l,n} = \frac{1}{N}\frac{\sin\left(\frac{\pi}{N}(2D+1)(n-l)\right)}{\sin\left(\frac{\pi}{N}(n-l)\right)} \\ \mathbf{A}_2 = \left(\tilde{\mathbf{H}}_{t,l}^{(i)}\tilde{\mathbf{H}}_{t,l}^{(i)^H}\right)^*\end{cases} \tag{4.9}$$

since from (3.3) we know that

$$\sum_{|k|\le D}e^{-j\Delta k} = \frac{\sin\left(\Delta\left(2D+1\right)/2\right)}{\sin\left(\Delta/2\right)}.$$

Thus $\tilde{\mathbf{b}}_\star$ is the principle eigenvector of $\mathbf{A}$ and

$$\mathbf{b}_\star = \mathrm{diag}(\sigma_w^2\mathbf{I}+\mathbf{H}_{t,l}^{(i)}\mathbf{H}_{t,l}^{(i)^H})^{-\frac{1}{2}}\tilde{\mathbf{b}}_\star \tag{4.10}$$

Fig. 4.2 illustrates the effect of $N$-point max-SINR windowing on a representative realization of $\mathcal{H}_{d,f}$ where the dot size is proportional to the coefficient log-magnitude.

## 4.4 Max-SINR Window: Approximation in Large-$N_h$ Case

The optimal window coefficients $\mathbf{b}_\star$ from (4.10), require the knowledge of the current channel coefficients (See (4.9)). The computational burden essentially lies in calculating the elements of matrix $\mathbf{A}_2$. We now seek a channel-independent approximation to (4.10). From (4.7) and (4.9), we see that $\mathbf{A}_2$ can be expanded into

$$\mathbf{A}_2 = \mathrm{diag}\left(\sigma_w^2\mathbf{I}+\mathbf{H}_{t,l}^{(i)}\mathbf{H}_{t,l}^{(i)^H}\right)^{-\frac{1}{2}}\left(\mathbf{H}_{t,l}^{(i)}\mathbf{H}_{t,l}^{(i)^H}\right)^*\mathrm{diag}\left(\sigma_w^2\mathbf{I}+\mathbf{H}_{t,l}^{(i)}\mathbf{H}_{t,l}^{(i)^H}\right)^{-\frac{1}{2}}$$

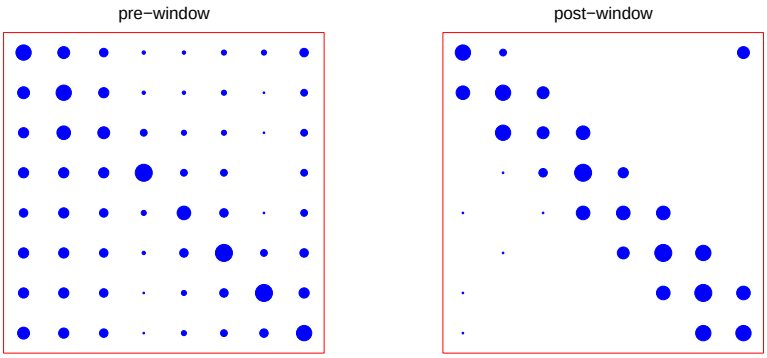


Figure 4.2: Typical effect of $N$-point max-SINR windowing on $\mathcal{H}_{d,f}$ coefficient magnitudes.

For channels that exhibit a large delay-spread (i.e., large $N_h$), we can approximate the summation in $\mathbf{H}_{t,l}^{(i)}\mathbf{H}_{t,l}^{(i)^H}$ using an expectations:

$$\begin{aligned}\left[\mathbf{H}_{t,l}^{(i)}\mathbf{H}_{t,l}^{(i)^H}\right]_{n,l} &\approx \mathrm{E}\left\{\sum_{m=0}^{N_h-1} h_{t,l}^{(i)}(n,m)h_{t,l}^{(i)^*}(l,m)\right\} \\ &= \sum_{m=0}^{N_h-1}\sigma_m^2 J_0\left(2\pi f_d(n-l)\right)\end{aligned}$$

where we used the property of $\mathrm{E}\{h_{t,l}^{(i)}(n,m)h_{t,l}^{(i)^*}(l,m)\}$ given by (3.1). The max-SINR window quantities then become

$$\begin{aligned}\mathbf{b}_\star &\approx \left(\sigma_w^2+\sum_{m=0}^{N_h}\sigma_m^2\right)^{-\frac{1}{2}}\tilde{\mathbf{b}}_\star \\ [\mathbf{A}_2]_{l,n} &\approx \frac{\sum_{m=0}^{N_h}\sigma_m^2}{\sigma_w^2+\sum_{m=0}^{N_h}\sigma_m^2}J_0\left(2\pi f_d(n-l)\right)\end{aligned}$$

As desired, an approximate max-SINR window can be constructed using channel and noise *statistics* rather than channel *realizations*. Furthermore, $\sigma_w^2$ and $\sigma_m^2$ only act to scale the window (and hence do not affect the resulting SINR). Thus the window coefficients essentially depend only on $f_d$, $D$ and $N$. This proves very beneficial from an implementation standpoint.

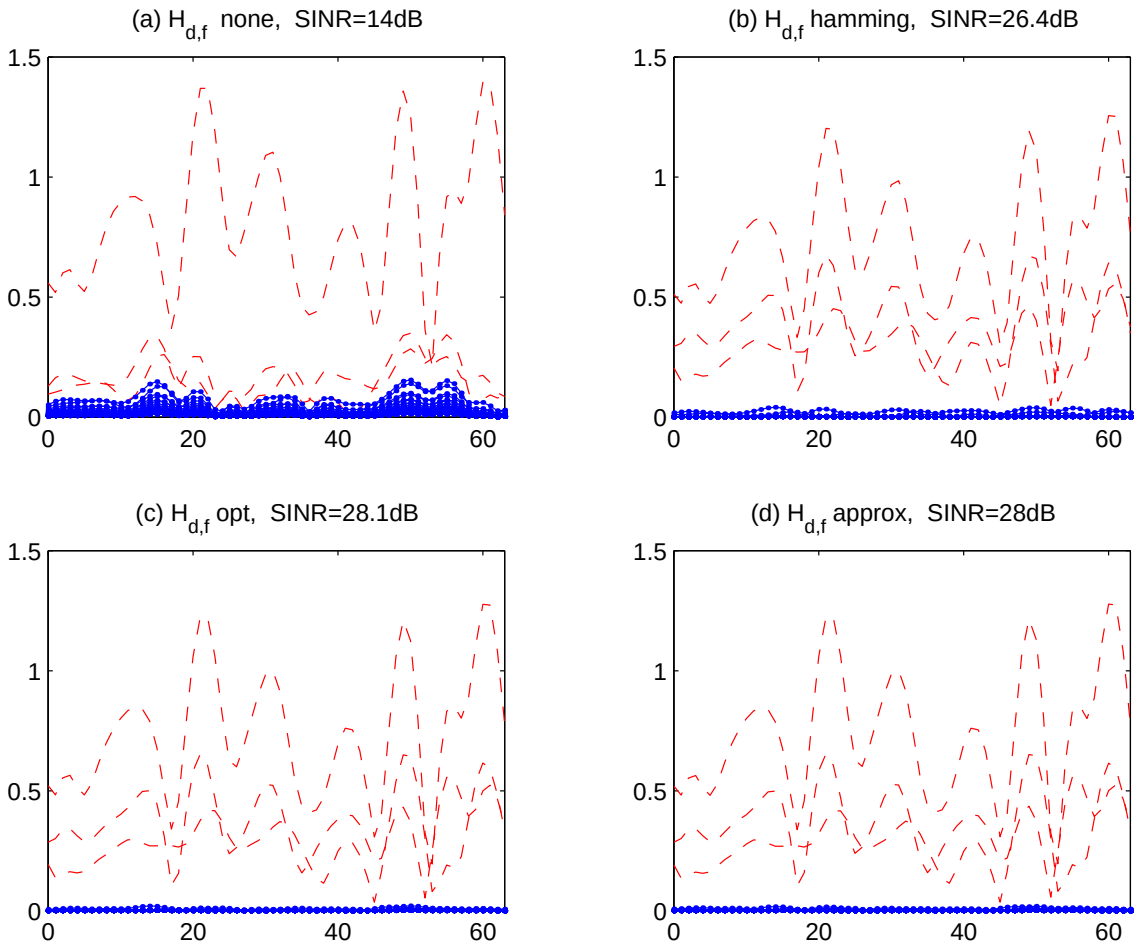


Figure 4.3: Example of the effects of windowing

Fig. 4.3 provides an example to observe the effects of windowing. We consider an OFDM system with $N = 64$, $N_h = 16$ and $f_d = 0.005$. We design the max-SINR window and the approximate max-SINR window for $D = 1$ at SNR = 30 dB and assume the mask operator preserves diagonals $\{-D, \ldots, D\}$. We use dotted lines to indicate the coefficients that are wrongfully assumed to be zero by the receiver (due to the masking operation). Note, these coefficients will contribute to the overall level of interference in the system. In Fig. 4.3 $(a)$ we consider an OFDM system that does not incorporate windowing. Observe, the magnitudes of the interference coefficients are significant and leads to a very low SINR value. In Fig. 4.3 $(b)$ we incorporate a Hamming window and observe that windowing manages to significantly reduce the extent of the ICI response. However, its not the best we can do as far as maximizing the SINR. In Fig. 4.3 $(c)$ & $(d)$ we incorporate max-SINR windowing and its realization-independent approximation respectively. The max-SINR window provides the highest value of SINR and its encouraging to observe a near-optimal performance by the approximate max-SINR window.

In Fig. 4.4, we plot SINR $(\mathcal{E}_s/\mathcal{E}_{ni})$ versus symbol-to-noise power ratio for an OFDM system with $N = 128, N_h = 32$, and various values of $f_d$. The benefits of windowing are clear. Observe that the max-SINR window and its realization-independent approximation have nearly identical performance.

In Fig. 4.5, we plot SINR $(\mathcal{E}_s/\mathcal{E}_{ni})$ versus the normalized Doppler spread for an OFDM system with $N = 128, N_h = 32$, and various values of SNR. For a given signal to noise ratio, the average SINR of the OFDM system decreases with increase in channel time variation (characterized by $f_d$). Observe that, the max-SINR windowed system has the highest SINR.

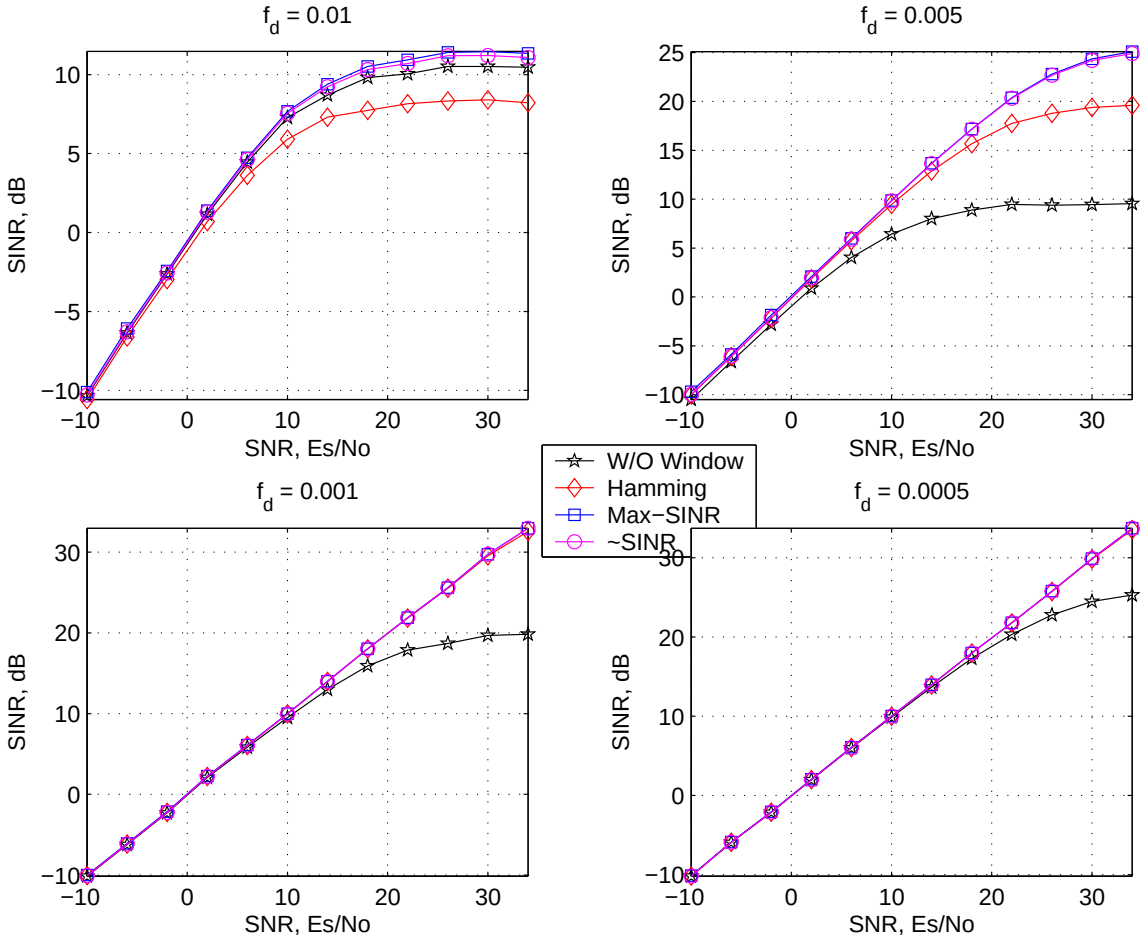


Figure 4.4: Post-windowing SINR ($\mathcal{E}_s/\mathcal{E}_{ni}$) versus Symbol-to-Noise Ratio ($E_s/N_o$)

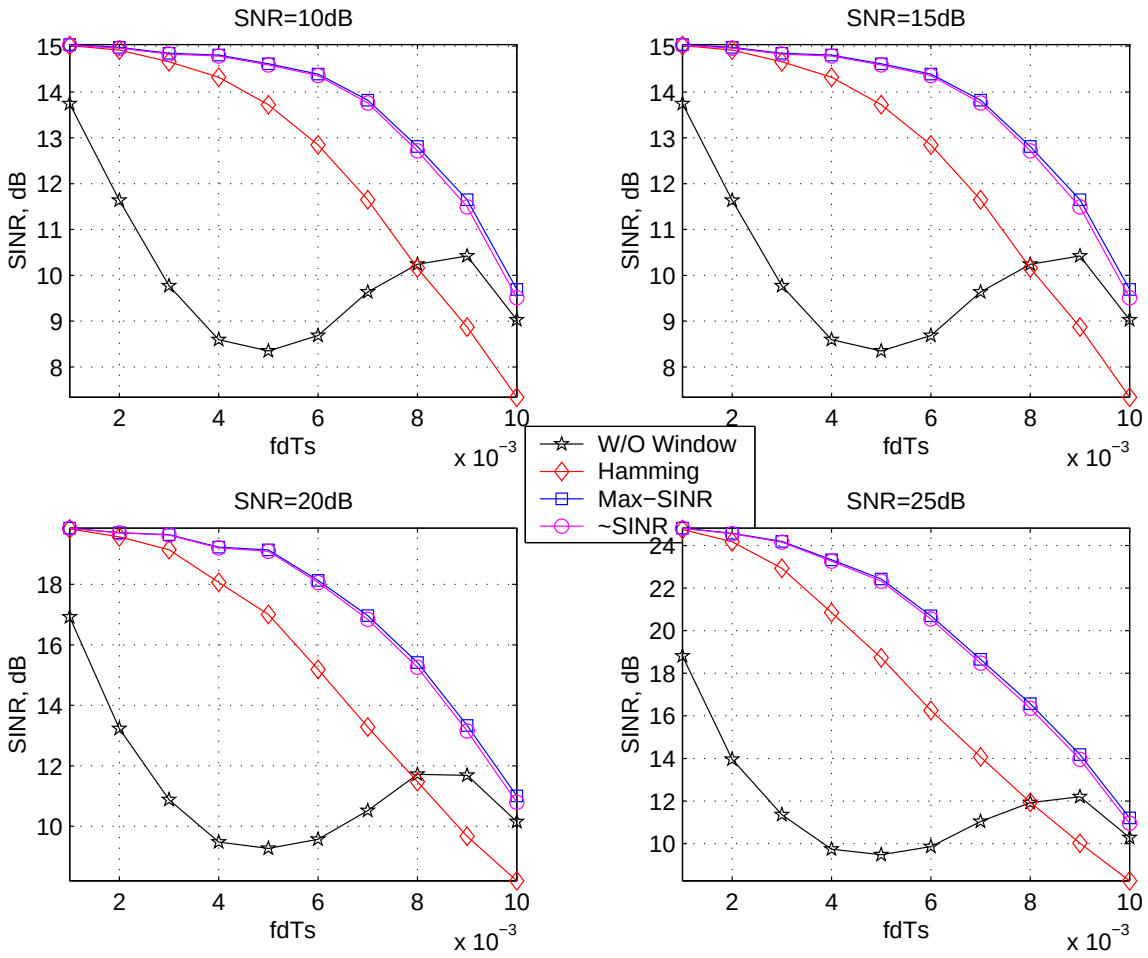


Figure 4.5: Post-windowing SINR ($\mathcal{E}_s/\mathcal{E}_{ni}$) versus Normalized Doppler Spread ($f_d$)

# CHAPTER 5

# SCHEMES FOR COHERENT ESTIMATION, DECODING & DETECTION IN OFDM

The process of detecting the transmitted symbols assuming perfect channel knowledge is called *coherent* detection. Since the end result we want to achieve is reliable data transmission, bit error rate (BER) minimization becomes the criterion for optimality of detection. In uncoded OFDM systems with i.i.d. symbols and noise, BER can be optimally minimized by maximum likelihood sequence detection (MLSD). The main drawback of MLSD is its exponential complexity. Suboptimal linear detection schemes involve generation of least-squares (LS) or linear minimum mean square error (LMMSE) soft-estimates for individual symbols followed by thresholding to produce hard symbol estimates. Though suboptimal, these techniques can be implemented with polynomial complexity. A major drawback of uncoded OFDM systems is their inability to exploit the *diversity* offered by the fading multipath channel since they will not reliably detect symbols transmitted on subcarriers that experience severe fading. Since OFDM is primarily used with channels that are fairly frequency-selective, we expect to encounter deep spectral nulls quite often. Thus practical OFDM systems must incorporate error control coding to exploit multipath diversity and overcome these drawbacks.

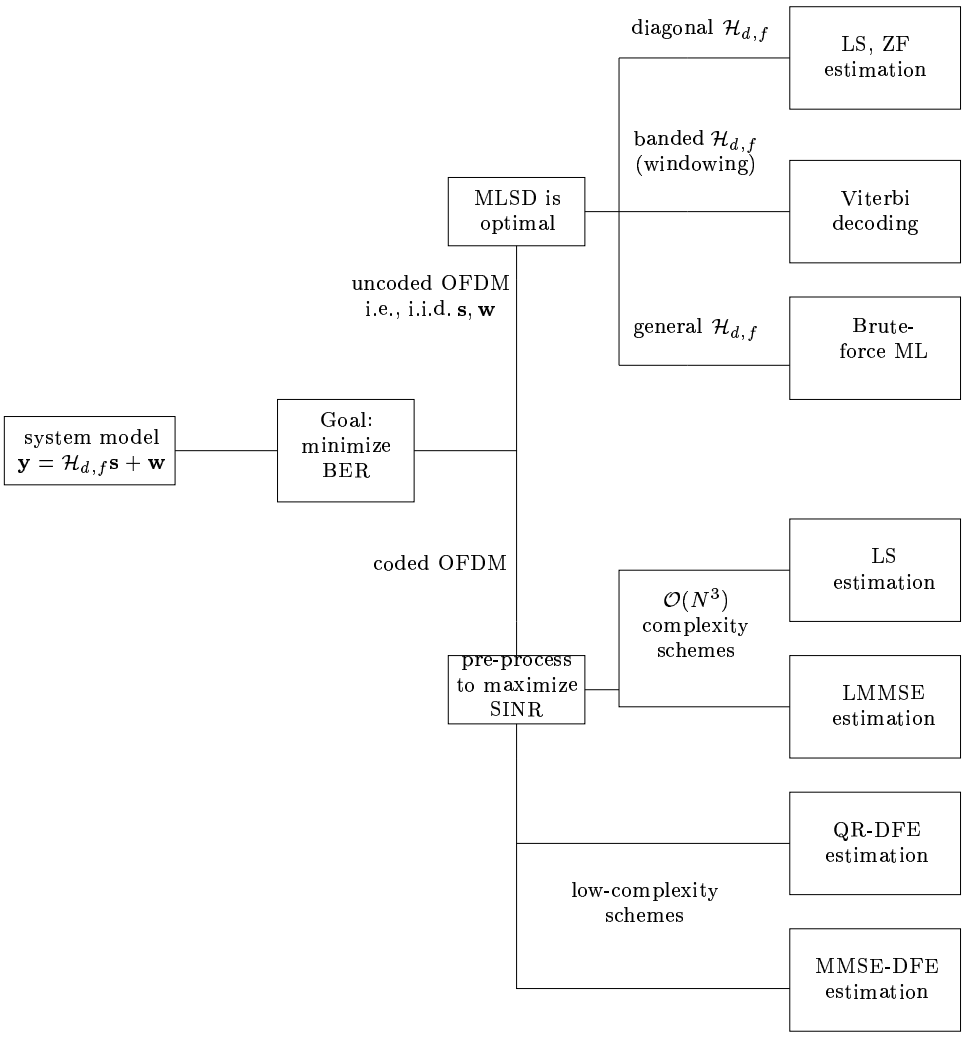


Figure 5.1: Overview of detection schemes for OFDM

In coded OFDM systems, usually, an estimation technique is used to obtain soft-estimates of the individual transmitted symbols. These soft-estimates are then fed to a decoder which outputs the hard symbol decisions. If we assume an OFDM system employing powerful error-control coding, then the final BER performance is proportional to the average SINR across carriers [36]. In Section 5.1 we review detection schemes for uncoded OFDM systems while in Section 5.2 we propose techniques to obtain soft-symbol-estimates for OFDM systems employing *powerful* coding.

## 5.1 Detection Schemes for Uncoded OFDM

From (2.11) we know that each block of an OFDM system can be expressed by the vector equation

$$\mathbf{y} = \mathcal{H}_{d,f}\mathbf{s} + \mathbf{w} \tag{5.1}$$

When the transmitted symbols ($\mathbf{s}$) and the noise ($\mathbf{w}$) are i.i.d. (i.e., the uncoded AWGN case), optimal detection of $\mathbf{s}$ from the observation vector $\mathbf{y}$ can be accomplished by maximum likelihood sequence detection (MLSD) (See Section 5.1.1). If windowing in employed to give $\mathcal{H}_{d,f}$ a sparse (banded) structure, then MLSD can be efficiently accomplished by the Viterbi algorithm [38] using path metrics determined by the non zero entries of $\mathcal{H}_{d,f}$. However, in general, if some sort of coding is employed (i.e., $\mathbf{s}$ is no longer i.i.d.) and/or windowing is employed (i.e., $\mathbf{w}$ is no longer i.i.d.), the Viterbi algorithm is no longer MLSD. Even so, the Viterbi algorithm may provide relatively good performance[5], especially if the complexity of a combined channel/code trellis can be tolerated. When the channel is LTI, $\mathcal{H}_{d,f}$ becomes diagonal

[5]In single-carrier systems, for example, noise correlation induced by ISI-shortening does not preclude the application of the Viterbi algorithm [12].

and MLSD reduces to a simple $\mathcal{O}(N)$ complexity zero-forcing equalization followed by thresholding (See Section 5.1.2)

### 5.1.1 General $\mathcal{H}_{d,f}$ (Brute-Force MLSD)

From (5.1), if $\mathcal{H}_{d,f}$ is known, the conditional probability density function of $\mathbf{y}$ given $\mathbf{s}$ is

$$p(\mathbf{y}|\mathbf{s}) = \frac{1}{(2\pi\sigma_w^2)^{\frac{N}{2}}} \exp\left(-\frac{1}{2\sigma_w^2}\|\mathbf{y} - \mathcal{H}_{d,f}\mathbf{s}\|^2\right) \tag{5.2}$$

Here we have assumed that $\mathbf{s}$ and $\mathbf{w}$ are uncorrelated and, in addition, $\mathbf{w} \sim \mathcal{N}(\mathbf{0}, \sigma_w^2\mathbf{I})$. The MLSD rule is given by,

$$\begin{aligned} \breve{\mathbf{s}} &= \arg \max_{\mathbf{s}\in\mathbf{S}} p(\mathbf{y}|\mathbf{s}) \\ &= \arg \min_{\mathbf{s}\in\mathbf{S}} \|\mathbf{y} - \mathcal{H}_{d,f}\mathbf{s}\|^2 \end{aligned} \tag{5.3}$$

where $\mathbf{S}$ denotes the set of all possible valid symbol vectors and (5.3) follows from (5.2). Thus MLSD involves a brute-force search over all possible $\mathbf{s} \in \mathbf{S}$ and the one that satisfies (5.3) is the solution. Clearly the complexity of detection is exponential in the length of $\mathbf{s}$ (i.e., $N$) making this technique highly impractical.

### 5.1.2 Diagonal $\mathcal{H}_{d,f}$

For LTI channels, $\mathcal{H}_{d,f}$ is diagonal and the (5.1) can be expressed as a set of decoupled equations

$$y_i = h_i s_i + w_i, \qquad i = 0, \ldots, N-1$$

Next we can rewrite (5.2) as

$$\begin{aligned} p(\mathbf{y}|\mathbf{s}) &= \frac{1}{(2\pi\sigma_w^2)^{\frac{N}{2}}} \exp\left(-\frac{1}{2\sigma_w^2}\sum_{i=0}^{N-1}|y_i - h_i s_i|^2\right) \\ &= \Pi_{i=0}^{N-1} p(y_i|s_i) \end{aligned}$$

since

$$p(y_i|s_i) = \frac{1}{\sqrt{2\pi\sigma_w^2}} \exp\left(-\frac{1}{2\sigma_w^2}|y_i - h_i s_i|^2\right).$$

Observe, the joint likelihood function is a product of marginal likelihood functions, thus finding the ML solution for $\mathbf{s}$ is equivalent to finding the ML solution for each $s_i$ individually. Clearly,

$$\begin{aligned} \breve{s}_i &= \arg \max_{s_i \in \mathbf{Q}} p(y_i|s_i) \\ &= \arg \min_{s_i \in \mathbf{Q}} |y_i - h_i s_i|^2 \end{aligned}$$

where $\mathbf{Q}$ is the set of QAM symbols. Clearly the ML solution for $s_i$ is obtained by thresholding $y_i/h_i$. With diagonal $\mathcal{H}_{d,f}$, the ML solution reduces to an element-by-element thresholding of $\mathcal{H}_{d,f}^{-1}\mathbf{y}$. Thus for the LTI channel case, ML detection is equivalent to a $\mathcal{O}(N)$ complexity zero-forcing equalization followed by thresholding.

## 5.2 Estimation Schemes for Coded OFDM

In coded single-carrier systems that face ISI, it is typical to employ time-domain equalization whose soft symbol estimates are then used for subsequent decoding. Typically, the ISI channels in single-carrier systems are slowly-varying from symbol to symbol, so that a fixed or tracking linear filter is effective for equalization. In our scenario, we obtain the soft symbol estimates through frequency-domain Doppler equalization of the ICI response. Since the ICI responses vary significantly from subcarrier to subcarrier (as in Fig. 3.1), we cannot rely on a similar filtering approach.

In Section 5.2.1 and Section 5.2.2 we formulate schemes to obtain soft symbol estimates which are optimal in the least-squares and minimum mean square error sense

respectively. Though easy to formulate these are highly impractical to implement due to their $\mathcal{O}(N^3)$ complexity.

As alternatives, we propose two computationally efficient schemes for soft symbol estimation which exploit the structure of the sparse post-windowed channel matrix. In Section 5.2.3 we outline a simple diversity exploiting QR-based decision-directed estimation scheme having $\mathcal{O}(D^2N)$ complexity ($D \ll N$) and in Section 5.2.4 we outline a MMSE-based decision-directed estimation scheme having a much better performance though at an increased $\mathcal{O}(D^3N)$ complexity.

### 5.2.1 Least-Squares Estimation

Recall from (2.11), each block of an OFDM system can be expressed by the vector equation $\mathbf{y} = \mathcal{H}_{d,f}\mathbf{s} + \mathbf{w}$. The least-squares (LS) estimate for the unknown symbols in $\mathbf{s}$ is given by

$$\tilde{\mathbf{s}}_{ls} = \arg \min_{\mathbf{s}} [(\mathbf{y} - \mathcal{H}_{d,f}\mathbf{s})^H(\mathbf{y} - \mathcal{H}_{d,f}\mathbf{s})]$$

Let $G = (\mathbf{y} - \mathcal{H}_{d,f}\mathbf{s})^H(\mathbf{y} - \mathcal{H}_{d,f}\mathbf{s})$, minimizing with respect to $\mathbf{s}$

$$\frac{\partial G}{\partial \mathbf{s}} = 2\mathcal{H}_{d,f}^H(\mathbf{y} - \mathcal{H}_{d,f}\mathbf{s}) = \mathbf{0}$$

and the LS estimate (assuming invertible $\mathcal{H}_{d,f}$) is

$$\tilde{\mathbf{s}}_{ls} = \mathcal{H}_{d,f}^{-1}\mathbf{y}$$

Thus, the LS estimator is equivalent to a zero-forcing (ZF) equalizer. These soft estimates are then fed to the decoder for subsequent decoding after which the hard symbol estimates are obtained. Clearly the main drawback of this estimation technique is the $\mathcal{O}(N^3)$ complexity of inverting the non-diagonal $N \times N$ channel matrix $\mathcal{H}_{d,f}$.

### 5.2.2 Linear Minimum Mean-Square Error Estimation

The linear minimum mean-square error (LMMSE) estimate for the unknown symbols in $\mathbf{s}$ is given by [39]

$$\hat{\mathbf{s}}_{lmmse} = R_{\mathbf{sy}} R_{\mathbf{yy}}^{-1} \mathbf{y}$$

where $\mathbf{s}$ is uncorrelated with noise $\mathbf{w}$ ( $\mathrm{E}\{\mathbf{s}\mathbf{w}^H\} = \mathbf{0}$) and $\mathcal{H}_{d,f}$ is known. $R_{\mathbf{sy}}$ denotes the cross-covariance matrix between $\mathbf{s}$ and $\mathbf{y}$ and $R_{\mathbf{yy}}$ denotes the auto-covariance matrix of $\mathbf{y}$. Thus,

$$\begin{aligned} R_{\mathbf{sy}} &= \mathrm{E}\{\mathbf{s}\mathbf{y}^H\} \\ &= \mathcal{H}_{d,f}^H \end{aligned}$$

where we assume $\mathrm{E}\{\mathbf{s}\mathbf{s}^H\} = \mathbf{I}$ and

$$\begin{aligned} R_{\mathbf{yy}} &= \mathrm{E}\{\mathbf{y}\mathbf{y}^H\} \\ &= \mathcal{H}_{d,f}\mathcal{H}_{d,f}^H + \sigma_w^2 \mathbf{I} \end{aligned}$$

where $\sigma_w^2$ denotes the variance of the elements in $\mathbf{w}$. Thus the LMMSE estimate is given by

$$\hat{\mathbf{s}}_{lmmse} = \mathcal{H}_{d,f}^H (\mathcal{H}_{d,f}\mathcal{H}_{d,f}^H + \sigma_w^2 \mathbf{I})^{-1} \mathbf{y} \tag{5.4}$$

and these soft estimates are used for subsequent decoding. The estimates obtained from the LMMSE estimator are more reliable than the LS estimator due to absence of noise enhancement inherent to ZF equalizers. However again, the main drawback of this estimation scheme is the $\mathcal{O}(N^3)$ complexity of matrix inversion in (5.4).

### 5.2.3 Diversity Exploiting QR-Estimation

#### QR-Decomposition of a Matrix

Every $m \times n$ matrix ($m \geq n$) $H$ can be expressed as the product of an $m \times m$ unitary matrix $Q$ and an $m \times n$ upper triangular matrix $R$

$$[H]_{m\times n} = [Q]_{m\times m}[R]_{m\times n}$$

This principle is known as the QR-decomposition of a matrix. More specifically,

$$\underbrace{\begin{bmatrix} \uparrow & \uparrow & & \uparrow \\ \mathbf{h}_1 & \mathbf{h}_2 & \dots & \mathbf{h}_n \\ \downarrow & \downarrow & & \downarrow \end{bmatrix}}_{H} = \underbrace{\begin{bmatrix} \uparrow & \uparrow & & \uparrow \\ \hat{\mathbf{q}}_1 & \hat{\mathbf{q}}_2 & \dots & \hat{\mathbf{q}}_m \\ \downarrow & \downarrow & & \downarrow \end{bmatrix}}_{Q} \underbrace{\begin{bmatrix} \|\mathbf{q}_1\| & \langle\hat{\mathbf{q}}_1, \mathbf{h}_2\rangle & \langle\hat{\mathbf{q}}_1, \mathbf{h}_3\rangle & \dots & \langle\hat{\mathbf{q}}_1, \mathbf{h}_n\rangle \\ & \|\mathbf{q}_2\| & \langle\hat{\mathbf{q}}_2, \mathbf{h}_3\rangle & \dots & \langle\hat{\mathbf{q}}_2, \mathbf{h}_n\rangle \\ & & \ddots & \dots & \vdots \\ & & & & \|\mathbf{q}_n\| \\ \cdots & \cdots & \cdots & \cdots & \cdots \\ & & \mathbf{0}_{m-n\times n} & & \end{bmatrix}}_{R}$$

where $\langle \mathbf{a}, \mathbf{b}\rangle = \mathbf{b}^H\mathbf{a}$, $\|\cdot\|$ denotes the vector norm, $\mathbf{h}_i \in \mathbb{C}^m$ and

$$\begin{aligned} \mathbf{q}_1 &= \mathbf{h}_1, \\ \mathbf{q}_k &= \mathbf{h}_k - \sum_{i=1}^{k-1} \langle\hat{\mathbf{q}}_i, \mathbf{h}_k\rangle\hat{\mathbf{q}}_i, \quad k = 2, \dots, m \\ \hat{\mathbf{q}}_i &= \frac{\mathbf{q}_i}{\|\mathbf{q}_i\|} \end{aligned}$$

#### Solving Algebraic Equations

A system of linear equations can be written in vector form as

$$[\mathbf{y}]_{m\times 1} = [H]_{m\times n}[\mathbf{x}]_{n\times 1}$$

Using the QR-decomposition technique explained above we have

$$\begin{aligned} [\mathbf{y}]_{m\times 1} &= [Q]_{m\times m}[R]_{m\times n}[\mathbf{x}]_{n\times 1} \\ \tilde{\mathbf{y}} &= Q^H\mathbf{y} = R\,\mathbf{x} \end{aligned} \tag{5.5}$$

We now proceed to solve for the elements in $\mathbf{x}$ from $\tilde{\mathbf{y}}, R$. The structure of $R$ makes it possible to solve for the $n^{th}$ element in $\mathbf{x}$ using only the $n^{th}$ element in $\tilde{\mathbf{y}}$ and $[R]_{n,n}$. Knowing the $n^{th}$ element of $\mathbf{x}$ and the elements $[R]_{n-1,n}$ and $[R]_{n-1,n-1}$ we can then solve for the $(n-1)^{th}$ element of $\mathbf{x}$. Proceeding in this fashion we can solve for all the elements in $\mathbf{x}$. This procedure is computationally-efficient because it did not require an $\mathcal{O}(n^3)$ complexity matrix inversion to solve for elements in $\mathbf{x}$ ($\mathbf{x} = H^{\dagger}\mathbf{y}$, $H^{\dagger} = (H^H H)^{-1} H^H$). However, we need to feedback the value of each detected element in $\mathbf{x}$ in order to solve for subsequent elements. Any wrong decisions fed back would jeopardize future decisions leading to the possibility of error-propagation; this is the main drawback of the decision-directed feedback technique.

**QR/Givens Decision-Directed Estimation**

In a nutshell, the goal of the signal processing described in Chapter 4 was to render an accurate "parsimonious" representation of the doubly-selective channel. Accuracy is ensured by max-SINR receiver pre-processing that yields an effectively sparse Doppler-frequency channel transfer function matrix $\mathcal{H}_{d,f}$. If we window the time-domain received signal prior to taking the FFT, the equivalent system can be expressed as (See (4.6))

$$\overline{\mathbf{y}} = \frac{1}{\sqrt{N}} \mathcal{C}(\mathbf{B}) \left( \mathcal{H}_{d,f} \mathbf{s} + \mathbf{w} \right)$$

Using the max-SINR technique suggested in Section 4.3 we can design the time-domain window coefficients $\mathbf{b}$ such that the matrix $\mathcal{C}(\mathbf{B})\mathcal{H}_{d,f}$ is sparse. Specifically we design the window to squeeze all the energy in the diagonals $\{-D, \ldots, D\}$. Next we apply the mask operator defined in Section 4.2 on $\mathcal{C}(\mathbf{B})\mathcal{H}_{d,f}$ to preserve only the diagonals $\{-D, \ldots, D\}$. We call this new matrix $\overline{\mathcal{H}}_{d,f}$ and its general structure is

seen in Fig. 5.2(a) where the shaded portion indicates the elements preserved by the mask operator $\mathcal{M}(\cdot)$. Thus the windowed OFDM system can be written in terms of

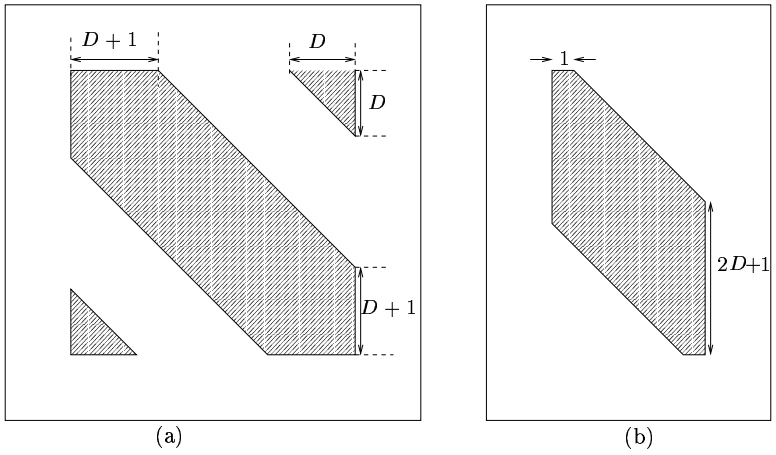


Figure 5.2: General structure of (a) the Doppler-frequency channel matrix after windowing and masking, (b) the Doppler-frequency channel matrix after windowing, masking and column deletion.

signal and noise-plus-interference components as

$$\overline{\mathbf{y}} = \overline{\mathcal{H}}_{d,f}\mathbf{s} + \overline{\mathbf{w}} \tag{5.6}$$

where

$$\begin{aligned} \overline{\mathcal{H}}_{d,f} &= \frac{1}{\sqrt{N}}\mathcal{M}(\mathcal{C}(\mathbf{B})\mathcal{H}_{d,f}) \\ \overline{\mathbf{w}} &= \frac{1}{\sqrt{N}}\left(\overline{\mathcal{M}}(\mathcal{C}(\mathbf{B})\mathcal{H}_{d,f})\mathbf{s} + \mathbf{w}\right). \end{aligned}$$

If the first $D$ and the last $D$ elements of $\mathbf{s}$ are known or suppressed pilots, the relationship between the unknown symbols $\mathbf{s}_u$ and the windowed frequency-domain observation vector $\overline{\mathbf{y}}^{(1)}$ (after pilot removal) can be written

$$\overline{\mathbf{y}}^{(1)} = \overline{\mathcal{H}}_{d,f}^{(1)}\mathbf{s}_u + \overline{\mathbf{w}}^{(1)} \tag{5.7}$$

where $\overline{\mathcal{H}}_{d,f}^{(1)}$ has the banded structure as seen in Fig. 5.2(b).

The general structure of $\overline{\mathcal{H}}_{d,f}^{(1)}$ makes it possible to obtain a soft-estimate of the last element in $\mathbf{s}_u$ using only the last element in $\overline{\mathbf{y}}^{(1)}$. After thresholding, the resulting hard symbol estimate could be fed back and used to detect the second-to-last element in $\mathbf{s}_u$, and so on.

However, if the lower diagonal entries in $\overline{\mathcal{H}}_{d,f}^{(1)}$ are small, the decisions made while detecting the last few elements in $\mathbf{s}_u$ would be unreliable. Any wrong decisions fed back could cause errors while detecting subsequent symbols. Leveraging diversity, we propose a QR-decomposition that annihilates the lowest diagonal in $\mathcal{H}_{d,f}^{(1)}$, producing a new system of equations given by

$$\overline{\mathbf{y}}^{(2)} = \overline{\mathcal{H}}_{d,f}^{(2)}\mathbf{s}_u + \overline{\mathbf{w}}^{(2)},$$

where,

$$\begin{aligned} \overline{\mathcal{H}}_{d,f}^{(2)} &= {Q^{(1)}}^H \overline{\mathcal{H}}_{d,f}^{(1)} \\ \overline{\mathbf{y}}^{(2)} &= {Q^{(1)}}^H \overline{\mathbf{y}}^{(1)} \end{aligned}$$

Continuing in this manner, we can remove the diagonals one at a time from the bottom, yielding a set of causal diversity models

$$\begin{aligned} \overline{\mathbf{y}}^{(i)} &= \overline{\mathcal{H}}_{d,f}^{(i)}\mathbf{s}_u + \overline{\mathbf{w}}^{(i)}, \qquad i = 1, \ldots, 2D+1 \\ \overline{\mathcal{H}}_{d,f}^{(i+1)} &= {Q^{(i)}}^H \overline{\mathcal{H}}_{d,f}^{(i)}, \qquad i = 1, \ldots, 2D \\ \overline{\mathbf{y}}^{(i+1)} &= {Q^{(i)}}^H \overline{\mathbf{y}}^{(i)}, \qquad i = 1, \ldots, 2D \end{aligned}$$

The structure of $\{\overline{\mathcal{H}}_{d,f}^{(i)}\}_{i=1}^{2D}$ actually enables us to perform each QR-decomposition via $\approx (N-2D)$ "Givens rotations" with a total of $\approx 4ND$ multiplies.

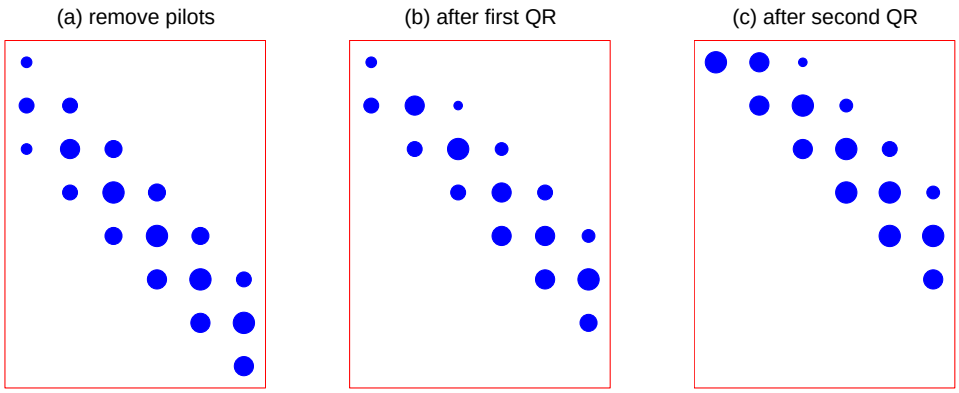


Figure 5.3: QR/Givens decision-directed diversity estimation

Fig. 5.3 illustrates the QR/Givens decision-directed diversity estimation strategy for $D = 1$. Fig. 5.3 (a) shows the general structure of $\overline{\mathcal{H}}_{d,f}^{(1)}$. Fig. 5.3 (b), (c) show the general structure of $\overline{\mathcal{H}}_{d,f}^{(2)}$ and $\overline{\mathcal{H}}_{d,f}^{(3)}$ obtained after the QR/Givens decomposition of $\overline{\mathcal{H}}_{d,f}^{(1)}$ and $\overline{\mathcal{H}}_{d,f}^{(2)}$ respectively.

These $(2D + 1)$ diversity models can be coherently combined to obtain the soft estimate of the last symbol in $\mathbf{s}_u$. This (tentative) decision can then be fed back so that the second-to-last symbol can be coherently estimated, and so on. Finally, all soft estimates would be sent to the decoder to obtain the hard symbol estimates.

Thus we observe that each symbol in $\mathbf{s}_u$ is estimated from a coherent combination of $(2D + 1)$ channel coefficients thereby exploiting diversity[6].

### 5.2.4 MMSE-based Decision-Directed Estimation

Assuming the same setup as in Section 5.2.3, from (5.7) we have

$$\overline{\mathbf{y}} = \overline{\mathcal{H}}_{d,f}\mathbf{s}_u + \overline{\mathbf{w}}$$

[6]The windowing followed by masking leads to a length $(2D + 1)$ ICI response.

where the superscript has been dropped for convenience and $\overline{\mathbf{w}}$ is a vector containing correlated Gaussian noise samples ($\overline{\mathbf{w}} \sim \mathcal{N}(\mathbf{0}, \sigma_w^2 \mathbf{C}\mathbf{C}^H)$, $\mathbf{C} = \mathcal{C}(\mathbf{B})$).

The structure of $\overline{\mathcal{H}}_{d,f}$ (See Fig. 5.2(b)) suggests that all information about the last element in $\mathbf{s}_u$ is contained in the $(2D+1)$ last elements of $\overline{\mathbf{y}}$. Thus we can set up the relation

$$\overline{\mathbf{y}}^{(1)} = \overline{\mathcal{H}}_{d,f}^{(1)} \mathbf{s}_u^{(1)} + \overline{\mathbf{w}}^{(1)}$$

where now $\overline{\mathbf{y}}^{(1)}, \mathbf{s}_u^{(1)}, \overline{\mathbf{w}}^{(1)}$ are the $(2D+1)$ last entries of $\overline{\mathbf{y}}, \mathbf{s}_u, \overline{\mathbf{w}}$ respectively and $\overline{\mathcal{H}}_{d,f}^{(1)}$ is the $(2D+1) \times (2D+1)$ upper triangular matrix formed by the last $(2D+1)$ rows and columns of $\overline{\mathcal{H}}_{d,f}$.

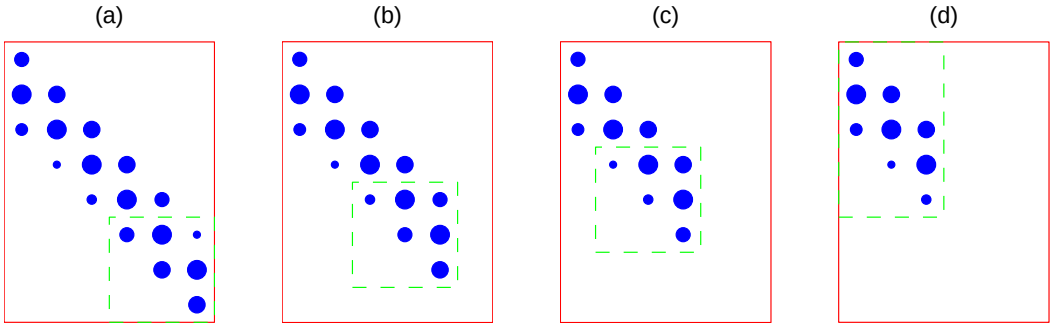


Figure 5.4: MMSE-based decision-directed estimation

Fig. 5.4(a) shows the basic structure of $\overline{\mathcal{H}}_{d,f}$ for $D = 1$ with the dashed region identifying the upper triangular matrix $\overline{\mathcal{H}}_{d,f}^{(1)}$. With channel knowledge, we can perform linear-MMSE estimation of the last element in $\mathbf{s}_u^{(1)}$ using an $\mathcal{O}(D^3)$ matrix inverse:

$$[\hat{\mathbf{s}}_u]_{2D+1} = \mathbf{e}_{2D+1}^H \, \overline{\mathcal{H}}_{d,f}^{(1)^H} \left( \overline{\mathcal{H}}_{d,f}^{(1)} \overline{\mathcal{H}}_{d,f}^{(1)^H} + \sigma_w^2 \mathbf{C}^{(1)} \mathbf{C}^{(1)^H} \right)^{-1} \overline{\mathbf{y}}^{(1)}$$

Above we used the fact that $\overline{\mathbf{w}}^{(1)} \sim \mathcal{N}(\mathbf{0}, \sigma_w^2 \mathbf{C}^{(1)} \mathbf{C}^{(1)^H})$, where $\mathbf{C}^{(1)}$ is a matrix containing the $(2D+1)$ last rows of $\mathbf{C}$ and $\mathbf{e}_{2D+1}$ is a length $(2D+1)$ unit vector given by $\mathbf{e}_{2D+1} = [0, \ldots, 0, 1]^H$.

Having estimated the last element in $\mathbf{s}_u$, a tentative decision can be fed back to remove the influence of this symbol. This involves canceling the symbol's contributions to $\overline{\mathbf{y}}$ using the last column of $\overline{\mathcal{H}}_{d,f}$ as shown in Fig. 5.4(b). Now the second-to-last element of $\mathbf{s}_u$ can be MMSE estimated using the same procedure. This process can be repeated until only the first $(2D+1)$ elements of $\mathbf{s}_u$ remain as shown in Fig. 5.4(d). These symbols can be jointly estimated using a linear MMSE scheme as follows: First we set up the relation

$$\overline{\overline{\mathbf{y}}} = \overline{\overline{\mathcal{H}}}_{d,f} \overline{\mathbf{s}}_u + \overline{\overline{\mathbf{w}}}$$

where $\overline{\overline{\mathbf{y}}}$ is a vector containing the $(4D+1)$ first elements of $\overline{\mathbf{y}}$ after canceling the contributions of the already detected symbols, $\overline{\overline{\mathcal{H}}}_{d,f}$ the $(4D+1) \times (2D+1)$ matrix indicated by the dashed region in Fig. 5.4(d) and $\overline{\overline{\mathbf{w}}}$ a vector containing correlated noise samples with $\overline{\overline{\mathbf{w}}} \sim \mathcal{N}(\mathbf{0}, \sigma_w^2 \overline{\overline{\mathbf{C}}}\, \overline{\overline{\mathbf{C}}}^H)$, where $\overline{\overline{\mathbf{C}}}$ is a matrix containing the $(4D+1)$ first rows of $\mathbf{C}$. The joint MMSE estimate of the unknown symbols is

$$\hat{\overline{\mathbf{s}}}_u = \overline{\overline{\mathcal{H}}}_{d,f}^H \, (\overline{\overline{\mathcal{H}}}_{d,f} \overline{\overline{\mathcal{H}}}_{d,f}^H + \sigma_w^2 \overline{\overline{\mathbf{C}}}\, \overline{\overline{\mathbf{C}}}^H)^{-1} \, \overline{\overline{\mathbf{y}}}$$

.

Here again, the MMSE estimates (soft-decisions) are saved at each step for subsequent decoding. This decision-directed MMSE scheme is expected to outperform the decision directed QR scheme from Section 5.2.3, though with an increased complexity of $\mathcal{O}(D^3 N)$ relative to $\mathcal{O}(D^2 N)$ multiplies. There are several ways to generalize this scheme. For example, incorporating more observations at each MMSE step would

generate better estimates but require larger matrix inverses. In addition iteration may prove worthwhile, for example, it is possible to re-compute the symbol estimates as soon as the first decoded version is available leading to a significant improvement in the estimates of the initial elements in $\mathbf{s}_u$.

# CHAPTER 6

# SIMULATION RESULTS

In Fig. 6.1 we plot the approximate BER performance for coded and uncoded OFDM in an LTI channel. We know that each OFDM block can be represented by the system of equations $y_i = h_i s_i + w_i$ where $i = \{0, \ldots N\}$ and $w_i \sim \mathcal{N}(0, \sigma_w^2)$. Thus for an uncoded OFDM system employing QPSK we have

$$P(e|h_i) = \frac{1}{2} \operatorname{erfc} \left( \sqrt{\frac{|h_i|^2}{2\sigma_w^2}} \right) \tag{6.1}$$

and we can approximate the BER for a block $P(e|H)$

$$P(e|H) = \frac{1}{N} \sum_{i=0}^{N-1} P(e|h_i) \tag{6.2}$$

where $H = \text{diag}(h_i)$. Next this BER can be averaged over a large number of blocks to yield the average BER of the system

$$P(e) = \text{E}[P(e|H)] = \text{E} \left\{ \frac{1}{N} \sum_{i=0}^{N-1} P(e|h_i) \right\} \tag{6.3}$$

Observe that the BER for an OFDM system is a function of the individual subcarrier SINRs. Any nulls in the channel spectrum would correspond to a low subcarrier SINR. From (6.1) we see that a low subcarrier SINR would translate to a high $P(e|h_i)$. These terms would dominate the sum in (6.2) and lead to an overall high system BER.

Thus for uncoded OFDM systems, the BER performance is dictated by the lowest subcarrier SINR. In general, for channels that are fairly frequency-selective, uncoded OFDM offers a poor BER performance.

For an OFDM system employing powerful coding, we can assume that the BER is a function of the average SINR across subcarriers [36] and so (6.2) becomes

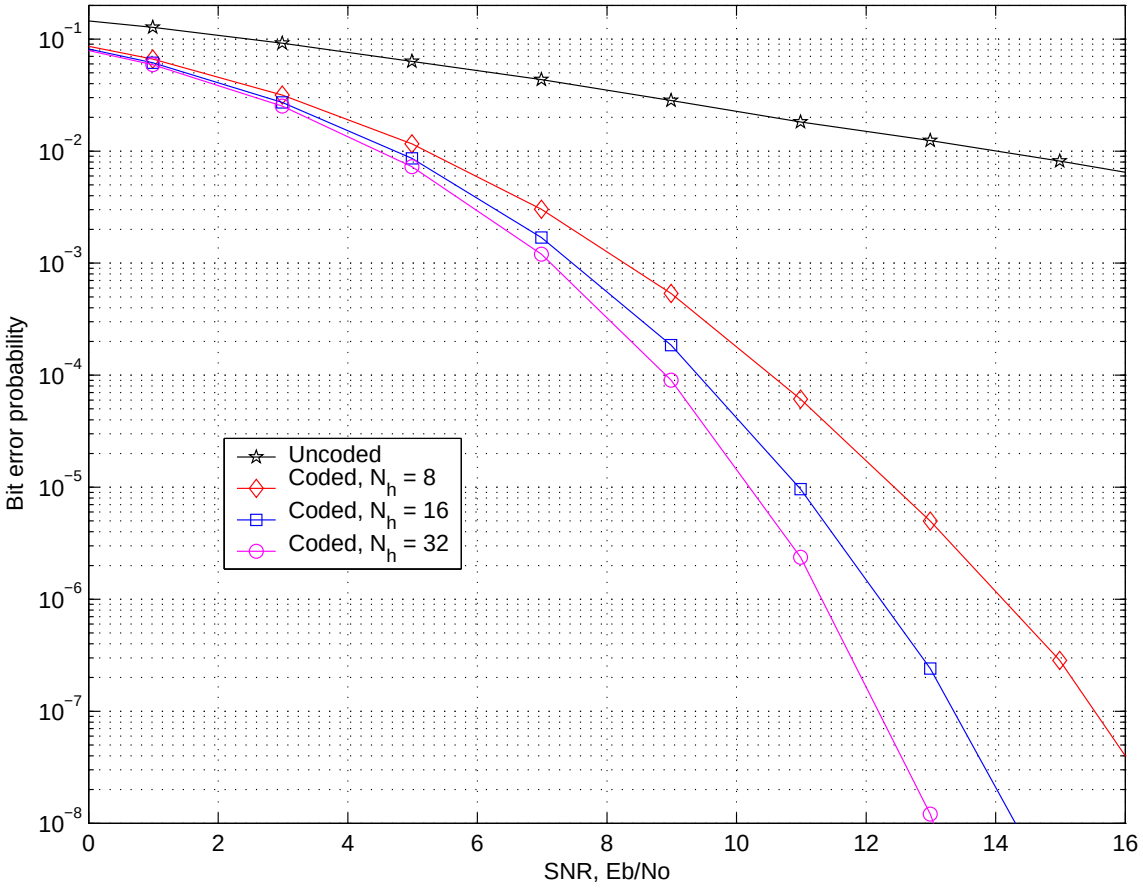


Figure 6.1: Uncoded versus coded OFDM in LTI channels

$$P(e|H) \approx \frac{1}{2}\text{erfc}\left(\sqrt{\frac{\sum_{i=0}^{N-1}|h_i|^2}{2N\sigma_w^2}}\right) \tag{6.4}$$

and the average BER can be calculated as in (6.3). Observe that the BER, though still a function of the individual subcarrier SINRs, is no longer dominated by the worst subcarrier SINR. This can be understood by the fact that, even though, some subcarriers have a low SINR, the average SINR over all the subcarriers is high enough, leading to a good BER performance. Further, since,

$$\mathrm{E}\left[\mathrm{erfc}(\cdot)\right] \geq \mathrm{erfc}\left(\mathrm{E}[\cdot]\right)$$

we can be sure that the BER obtained from (6.4) will always be less than or equal to that obtained from (6.2). With increase in channel delay spread $N_h$, there is diversity offered by the multipath channel. Simulation results show that BER for the coded OFDM system improves with the increase in channel delay spread $N_h$, thus exploiting diversity. This is the primary motivation for the use of channel coding in OFDM systems.

In Fig. 6.2 we plot the approximate BER performance of the detection schemes described in Section 5.2. The OFDM system employed QPSK and block length $N = 128$. The channel was WSSUS Rayleigh with delay spread $N_h = 32$ and normalized Doppler $f_d = 0.01$ in $(a)$ and $f_d = 0.001$ in $(b)$. Bit error probability was calculated as follows. First Jakes' method was used to generate fading channel realizations over a span of many blocks. For *each* block, the SINRs of symbol estimates were computed at each subcarrier using the different estimation techniques discussed in Section 5.2. Next the SINRs were averaged over the $N$ subcarriers, and then converted to BER assuming Gaussian interference and a QPSK decision mechanism

$$P(e|\mathcal{H}_{d,f}) \approx \frac{1}{2}\,\mathrm{erfc}\left(\sqrt{\frac{\mathrm{E[SINR]}}{2}}\right).$$

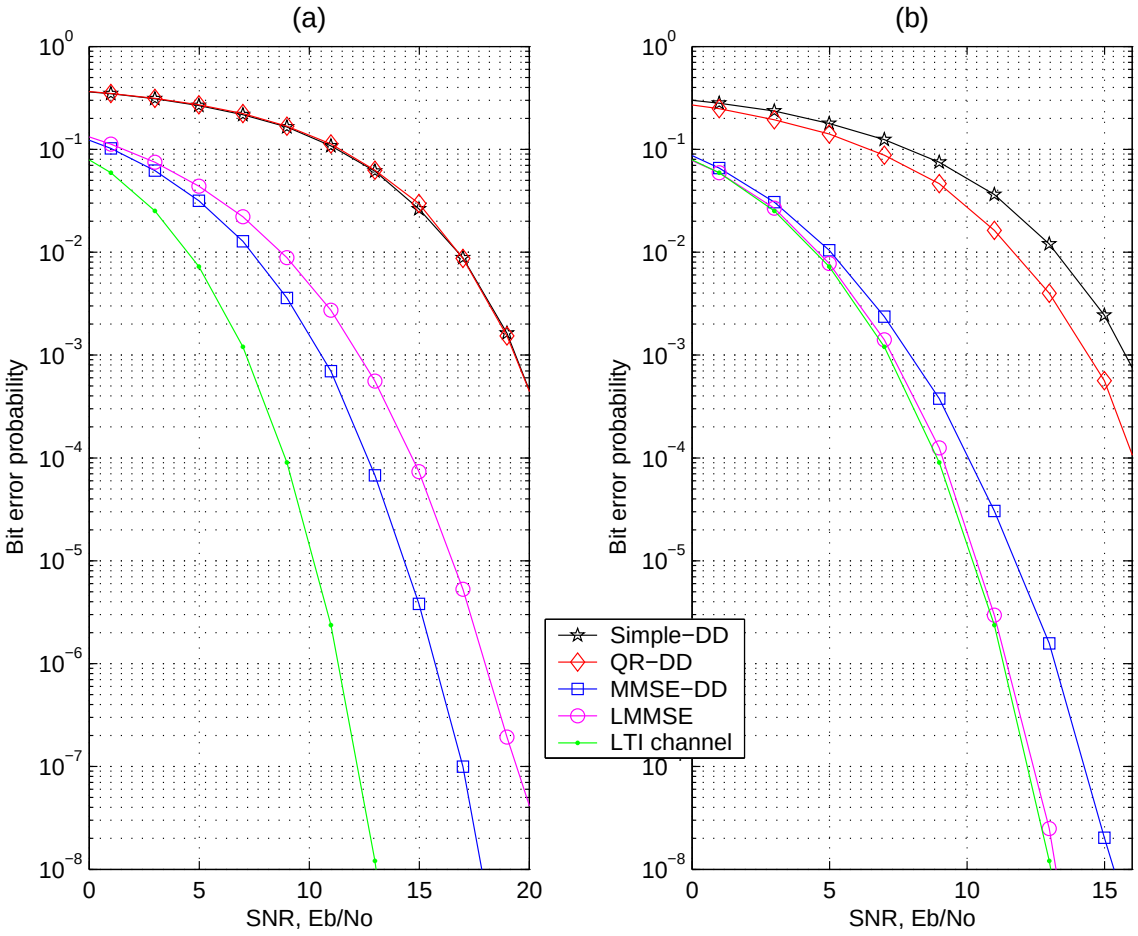


Figure 6.2: Comparison of different detection schemes for coded OFDM

Finally, these BERs were averaged over a large number of blocks. As discussed previously, carrier-averaging of SINR was employed to mimic the use of powerful coding. The "LTI channel" traces in Fig. 6.2 were included as a reference; they reflect the case where the channel remains fixed throughout each block but changes between blocks. The LTI channel trace indicates the best BER performance that can be expected from the coded OFDM system in a LTI multipath channel with delay spread $N_h = 32$. It is encouraging to observe that the low-complexity schemes described in Section 5.2.3 and Section 5.2.4 offer good performance relative to the optimal LTI channel trace.

Next, we proceed to take a closer look at some of the traces from Fig. 6.2 to support the claims we made in Chapter 5. In Section 5.2.3 we argued that the soft-symbol estimates obtained by the QR diversity exploiting technique were more reliable than the simple decision feedback technique. In Fig. 6.3 we plot the approximate BER performance of the two for an OFDM system employing QPSK with block length $N = 128$. The channel was WSSUS Rayleigh with delay spread $N_h = 32$ and normalized Doppler $f_d = 0.01$ in $(a)$ and $f_d = 0.001$ in $(b)$. Max-SINR windowing was employed with $D = 2$ in $(a)$ and $D = 1$ in $(b)$. Fig. 6.3 demonstrates that the $\mathcal{O}(D^2N)$ complexity QR technique outperforms the $\mathcal{O}(N)$ simple decision technique when $f_d = 0.001$ while they both provide the same performance at $f_d = 0.01$.

In Fig. 6.4 we plot the BER performance of the QR-based decision feedback estimator and the MMSE-based decision feedback estimator for an OFDM system employing QPSK with block length $N = 128$. The channel was WSSUS Rayleigh with delay spread $N_h = 32$ and normalized Doppler $f_d = 0.01$ in $(a)$ and $f_d = 0.001$ in $(b)$. Max-SINR windowing was employed to shorten the ICI responses to $D = 2$ in $(a)$ and

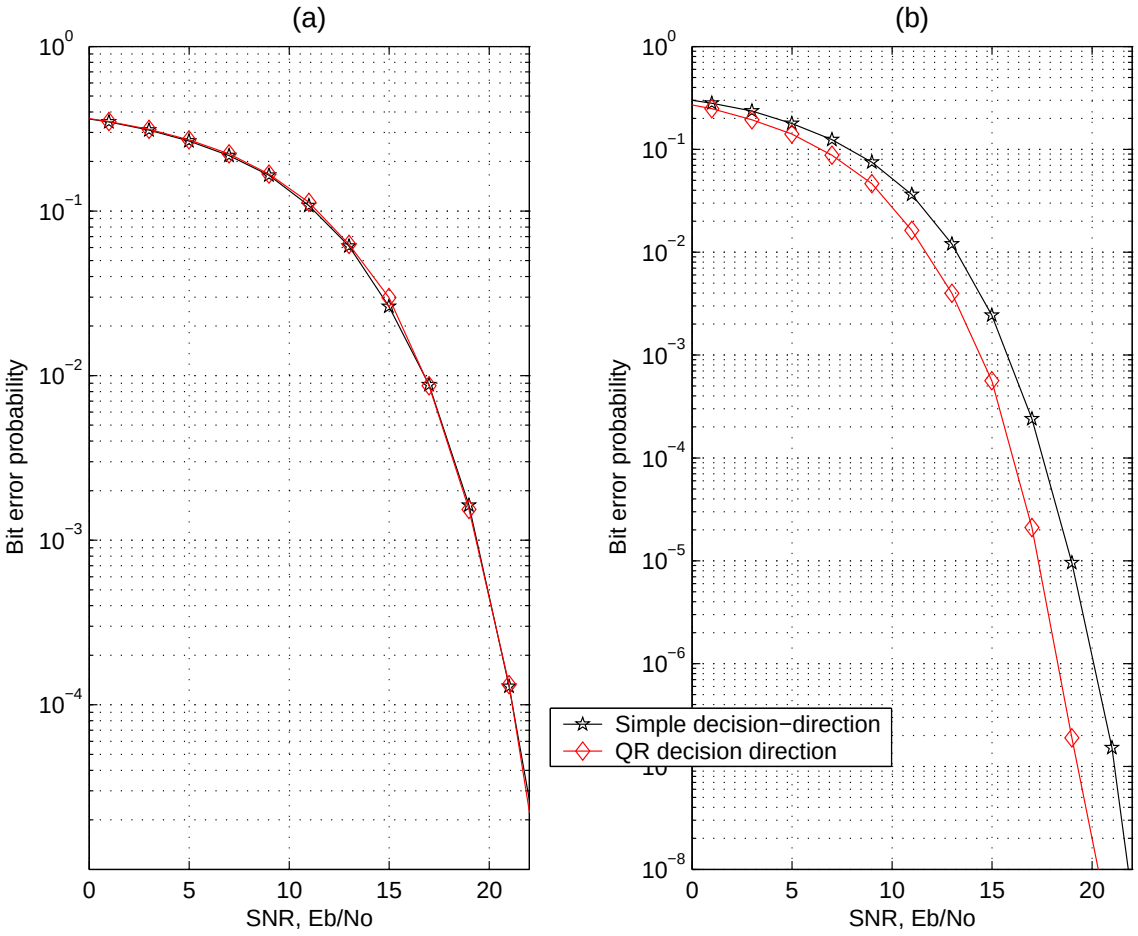


Figure 6.3: QR diversity decision feedback versus simple decision feedback

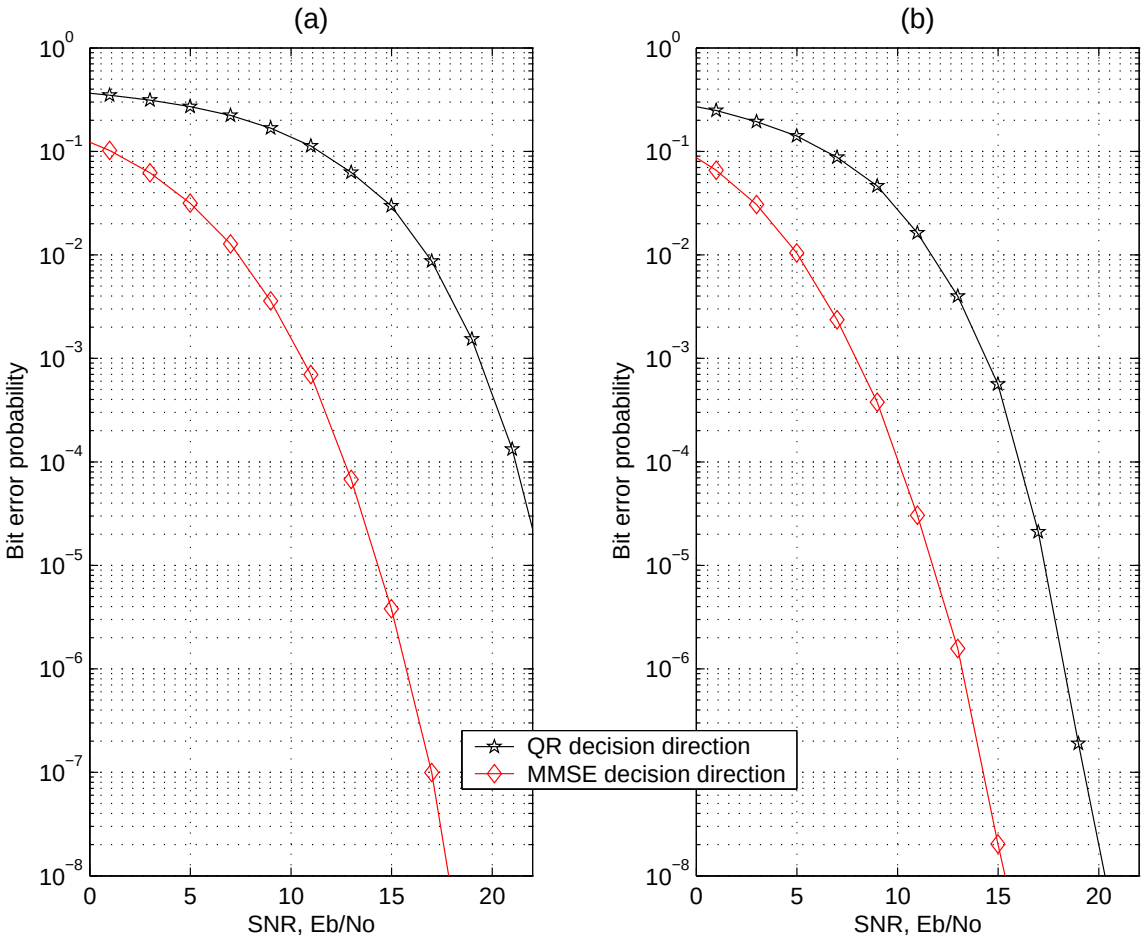


Figure 6.4: QR diversity decision feedback versus MMSE-based decision feedback

$D = 1$ in $(b)$. Fig. 6.4 demonstrates that the MMSE-based scheme far outperforms the QR-based scheme at a modest increase in complexity of $\mathcal{O}(D^3N)$ as opposed to $\mathcal{O}(D^2N)$ multiplies.

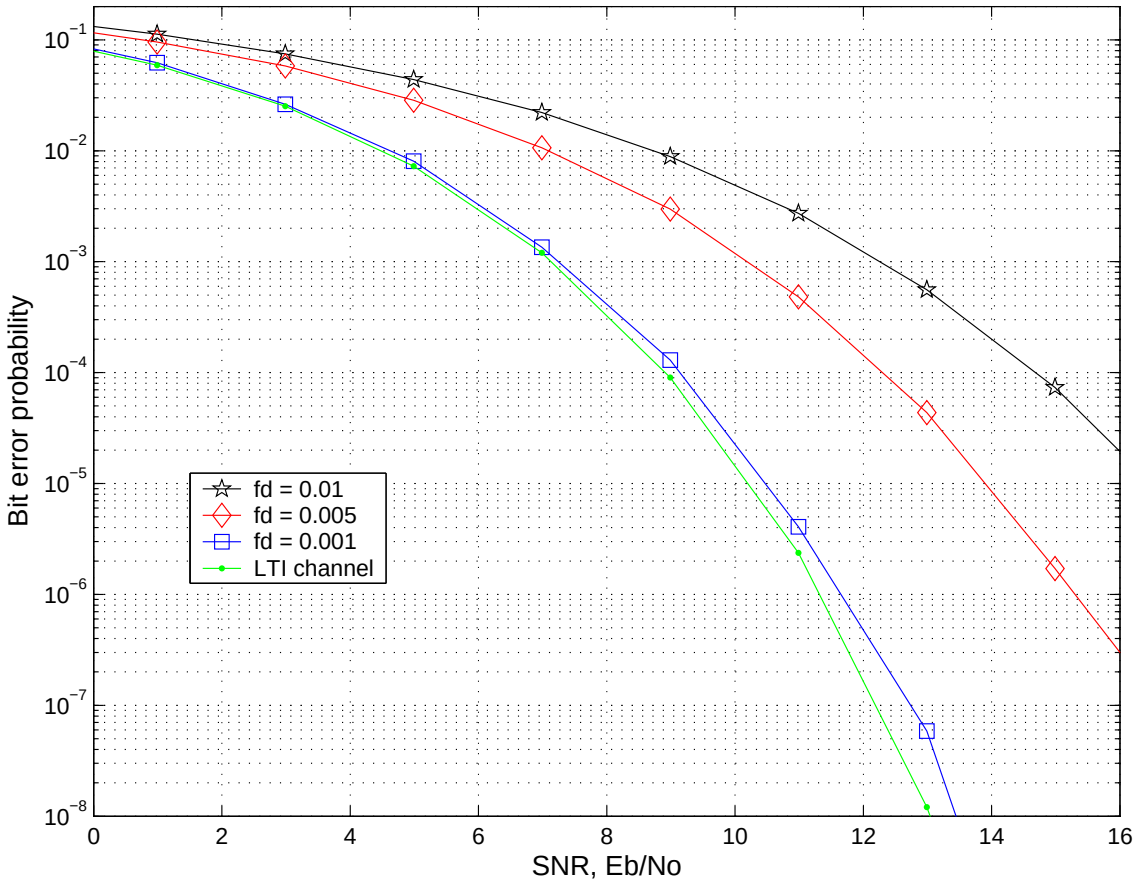


Figure 6.5: BER performance of the LMMSE detector versus normalized Doppler spread $f_d$

In Fig. 6.5 and Fig. 6.6 we plot the performance of the $\mathcal{O}(N^3)$ linear MMSE detector (Section 5.2.2) and the $\mathcal{O}(D^3N)$ MMSE-based decision-feedback detector

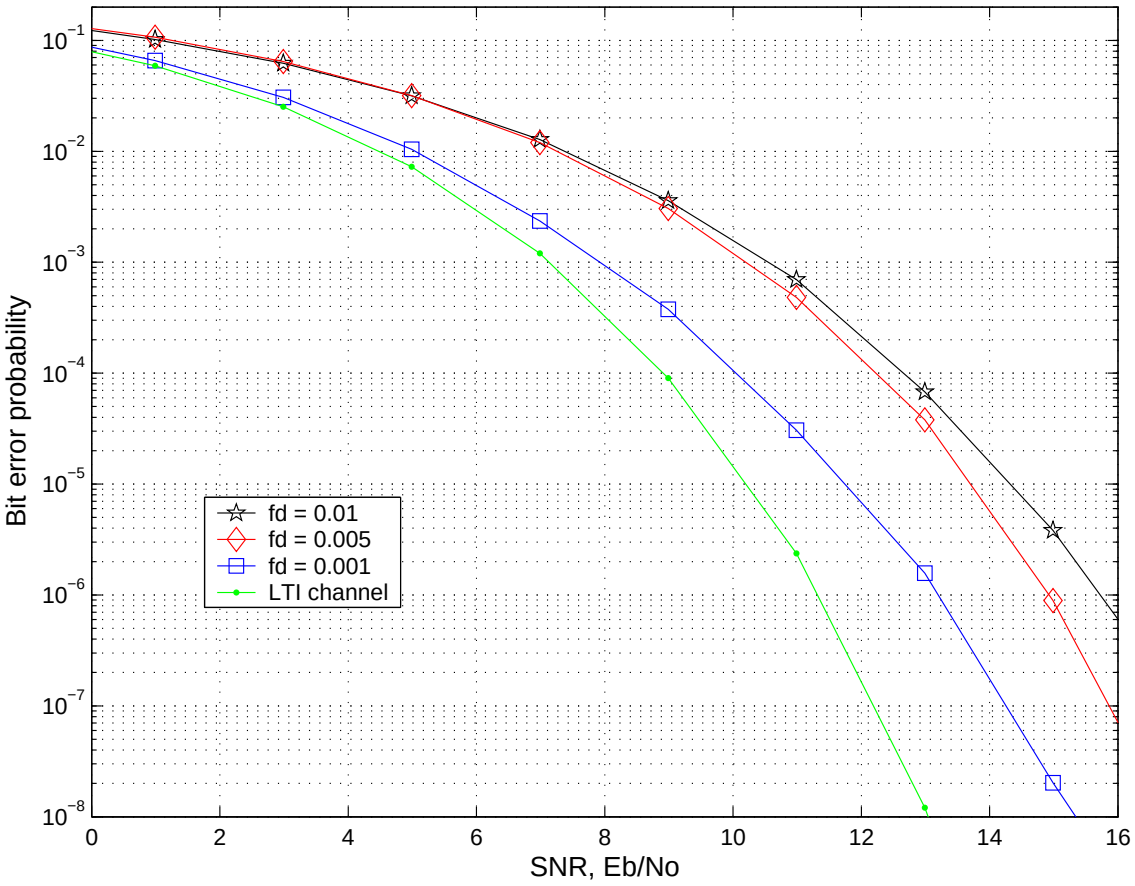


Figure 6.6: BER performance of the MMSE-based decision feedback detector versus normalized Doppler spread $f_d$

(Section 5.2.4) respectively for various Doppler spread $f_d$. The trend suggests a performance degradation with increase in channel time-variation.

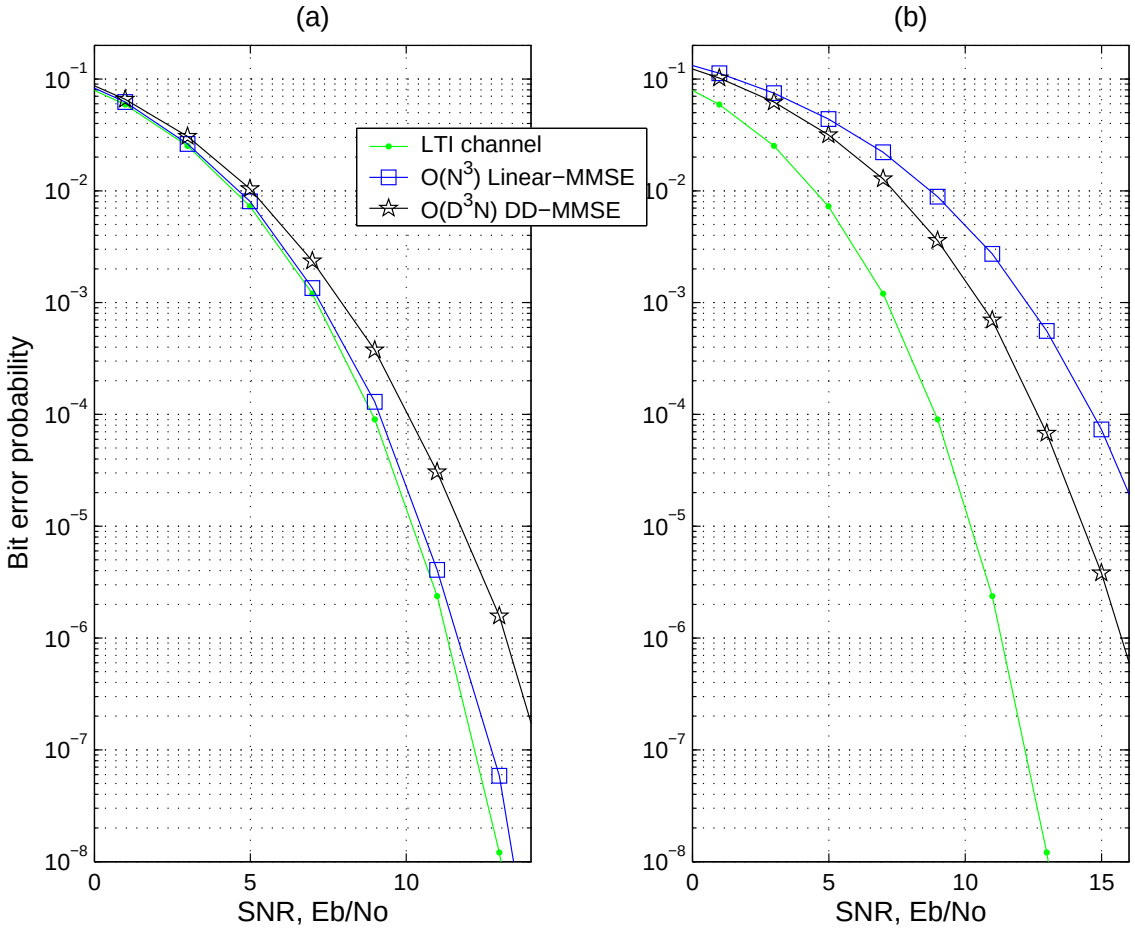


Figure 6.7: Comparison of the LMMSE detector and the MMSE-based decision feedback detector

Fig. 6.7 demonstrates that the MMSE-based decision-feedback scheme offers good performance relative to the linear MMSE detector. When $f_d = 0.001$, as seen in $(b)$, the $\mathcal{O}(N^3)$ linear detector outperforms the $\mathcal{O}(D^3N)$ decision-feedback detector at the cost of a much greater complexity. When $f_d = 0.01$, as seen in $(a)$, however, the

decision-feedback detector outperforms the linear detector even though the former is simpler to implement! This can be understood by the fact that the decision-feedback detector employs non-linear processing to leverage receiver knowledge of the finite-alphabet constellation.

# CHAPTER 7

# CONCLUSIONS & FUTURE WORK

In this thesis, we have addressed problems faced by OFDM systems in channels that are time- and frequency-selective. Perhaps the single largest impediment to reliable communication in a doubly-selective channel is interference in the form of ICI and/or ISI. In Chapter 3 we derived expressions to quantify the extent of ICI power as a function of other system parameters. These results suggested that, ICI power was prominent over nearby subcarriers and not so significant as we moved to distant subcarriers. Even then, neglecting distant-subcarrier ICI was detrimental to system performance while incorporating its effects lead to problems with implementation. As an alternative, we suggested a low-complexity linear receiver pre-processing strategy (i.e., max-SINR windowing) that optimally reduced the extent of ICI in the system. Finally we proposed low-complexity estimation schemes that exploit the post-windowed sparse ICI response to obtain reliable soft-symbol estimates. Simulation results clearly indicate good performance relative to standard detection schemes but with significant computational savings. As this thesis summarizes preliminary research in this area there are a number of avenues for future work.

### Enhanced Receiver Pre-processing

In Chapter 4 we proposed the design of a basic $N$-point max-SINR window to optimally reduce the extent of ICI power. Given that multipath channels typically exhibit an exponentially decaying delay profile [35], it is likely that a small amount of interblock interference (IBI) can be traded for a larger reduction in ICI. Thus, an improved strategy would involve windowing a $N+N_p+N_h$-point segment of the received signal, where $N_p$ denotes the cyclic-prefix length and $N_h$ the channel delay spread. Furthermore, viewing these windowing operations as diagonal matrix multiplication, we presume that banded matrix multiplication, or *super-windowing*, may offer yet improved performance at a relatively small increase in complexity. As future work, we could derive expressions for $> N$-point max-SINR windows, super-windows, and their realization-independent approximations. The extension to multiple transmit and/or receive antennas could be also considered.

In practice, max-SINR window coefficients may be inconvenient to compute because, e.g., the channel coefficients $\mathbf{H}_{t,l}$ might be unavailable or the computation of the principle eigenvector (See Section 4.3) may be too expensive. Furthermore, if the channel does not satisfy the Rayleigh assumption or the noise variance and Doppler spread are unknown, then direct computation of the realization-independent approximation will not be possible either. In these cases, it should still be feasible to determine the max-SINR window coefficients *automatically* using decision-directed or even blind adaptive techniques. Thus as future work it would be interesting to investigate adaptive algorithms to design schemes for max-SINR window coefficient adaptation.

### Low-Complexity Channel Estimation Algorithms

Since detection strategies often rely on knowledge of the channel coefficients, computationally-efficient channel estimation algorithms should be investigated. For OFDM in doubly-dispersive channels, significant time-variation increases both the number of channel parameters that must be estimated as well as the difficulty of estimating these parameters. As mentioned before, there exists relatively little work on doubly-selective channel estimation in a multicarrier context, and the existing approaches are not not practical for typical block lengths. As future work, it would be interesting to investigate pilot-based/blind LTV channel estimation, including performance analysis and extensions to multiple-antenna systems for the parsimonious channel representations used in this thesis. Note that blind multicarrier algorithms have recently been derived for the LTI case based on finite-alphabet [40], subspace [41] and cyclostationarity [42] ideas.

### Coding for Diversity Gain

From Fig. 6.1 it is evident that OFDM systems must employ some sort of channel coding techniques in order to exploit the diversity offered by the multipath fading channel. In this thesis we generated BER plots under the assumption that for coded OFDM systems the BER is a function of the average SINR across subcarriers. As future work, the effect of practical coding schemes that go hand-in-hand with more sophisticated detection algorithms (e.g., "turbo" methods) could be studied. In single carrier systems coding techniques are known to exploit the frequency-diversity offered by the ISI channel to improve BER performance. Thus coding schemes should be

derived that can exploit both the frequency- and temporal-diversity diversity that the doubly-selective channel has to offer.

### Differential Detection

Differential detection (DD) [10] is useful when coherent detection, with its reliance on channel knowledge, becomes impractical. DD has been applied to OFDM under time-domain differential modulation (TDDM), where information is coded into each subcarrier's inter-block differences, or frequency-domain differential modulation (FDDM), where information is coded into each block's inter-carrier differences [43]. To our knowledge, DD-OFDM has been proposed only for the slowly-fading case, i.e., where intra-block channel variation is negligible. There its has been shown that TDDM performs better than FDDM when channel variation across blocks is less than channel variation across carriers, and vice-versa [44].

In doubly-selective channels, DD-OFDM is complicated by the presence of ICI. As future work it would be interesting to investigate DD-OFDM algorithms for this case that leverage work on DD for single-carrier ISI channels (e.g., [45,46]). The hope is that the increased detection complexity (relative to coherent) would be offset by avoidance of channel estimation.

# APPENDIX A

# OFDM IN LTI CHANNELS

Assume that the time-domain received signal $r^{(i)}(n)$ is a noise corrupted and linearly distorted version of $x^{(i)}(n)$ as a consequence of a LTI channel with impulse response $h^{(i)}(m)$. The channel is assumed constant over the $i^{th}$ block. If the channel is causal with a maximum impulse response duration $N_h$, where $N_h \leq N_p \leq N$, then

$$r^{(i)}(n) = \sum_{m=0}^{N_h-1} h^{(i)}(m)x^{(i)}(n-m) + \tilde{w}_n^{(i)}, \quad n \in \{0, \ldots, N-1\} \tag{A.1}$$

The adequate length of the cyclic prefix enables the values of $x^{(i)}(n-m)$ in (A.1) to be well defined. We assume that $\tilde{w}_n^{(i)}$ are zero-mean white and Gaussian with variance $\sigma_w^2$. At each block $i$, the receiver drops the samples corresponding to the cyclic-prefix and applies $\{r^{(i)}(n)\}_{n=0}^{N-1}$ to a discrete Fourier transform (DFT), yielding $\{y_\nu^{(i)}\}_{\nu=0}^{N-1}$

$$y_\nu^{(i)} = \frac{1}{\sqrt{N}} \sum_{n=0}^{N-1} r^{(i)}(n) e^{-j\frac{2\pi\nu}{N}n}$$

We can relate $s_k^{(i)}$ to $y_\nu^{(i)}$ using the system equations (2.7), (A.1)

$$\begin{aligned}
y_\nu^{(i)} &= \frac{1}{\sqrt{N}} \sum_{n=0}^{N-1} \left( \sum_{m=0}^{N_h-1} h^{(i)}(m) \left[ \frac{1}{\sqrt{N}} \sum_{k=0}^{N-1} s_k^{(i)} e^{j\frac{2\pi(n-m)}{N}k} \right] + \tilde{w}_n^{(i)} \right) e^{-j\frac{2\pi\nu}{N}n} \\
&= \frac{1}{\sqrt{N}} \sum_{n=0}^{N-1} \tilde{w}_n^{(i)} e^{-j\frac{2\pi\nu}{N}n} + \sum_{k=0}^{N-1} s_k^{(i)} \left( \frac{1}{\sqrt{N}} \sum_{m=0}^{N_h-1} h^{(i)}(m) e^{-j\frac{2\pi k}{N}m} \right) \left( \frac{1}{\sqrt{N}} \sum_{n=0}^{N-1} e^{-j\frac{2\pi(\nu-k)}{N}n} \right) \\
&= w_\nu^{(i)} + \sum_{k=0}^{N-1} s_k^{(i)} (\tilde{H}_k^{(i)}) (\sqrt{N}\delta_{\nu-k}) \\
&= w_\nu^{(i)} + s_\nu^{(i)} H_\nu^{(i)}
\end{aligned} \tag{A.2}$$

The $w_\nu^{(i)}$ are statistically equivalent to their time-domain counterparts. Each $y_\nu^{(i)}$ in the $i^{th}$ block contains information about only the corresponding $s_\nu^{(i)}$, i.e., ICI is absent. In vector form (A.2) can be written as

$$\mathbf{y}^{(i)} = \mathcal{H}^{(i)}\mathbf{s}^{(i)} + \mathbf{w}^{(i)}$$

where $\mathcal{H}^{(i)}$ is a diagonal matrix that represents the frequency-domain effect of the channel and has $H_\nu^{(i)}$ as its individual entries. Knowing $\mathbf{y}^{(i)}$ and $\mathcal{H}^{(i)}$, MMSE detection of the unit variance QAM symbols in $\mathbf{s}^{(i)}$ is accomplished by element-by-element thresholding of the vector

$$\hat{\mathbf{s}}_{\text{mmse}}^{(i)} = \mathcal{H}^{(i)\,H}(\mathcal{H}^{(i)}\mathcal{H}^{(i)\,H} + \sigma_w^2\mathbf{I})^{-1}\mathbf{y}^{(i)}$$

Since $\mathcal{H}^{(i)}$ is diagonal, the matrix inversion required in the MMSE detection is trivial. This is the classical motivation for cyclic-prefix OFDM.

# BIBLIOGRAPHY


[1] Special Issue on, "Wireless broadband communications systems", IEEE Communications Magazine, Jan 1997.

[2] A.M. Sayeed and B. Aazhang, "Joint multipath-doppler diversity in mobile wireless communications", *IEEE Trans. on Communications*, vol. 47, pp. 123–132, Jan. 1999.

[3] N.J. Baas and D.P. Taylor, "Matched filter bounds for wireless communication over rayleigh fading dispersive channels", *IEEE Trans. on Communications*, vol. 49, pp. 1525–1528, Sept. 2001.

[4] S.U.H. Qureshi, "Adaptive equalization", *Proceedings of the IEEE*, vol. 73, pp. 1349–1387, Sept. 1985.

[5] H. Sari, G. Karam, and I. Jeanclaude, "Frequency-domain equalization of mobile radio and terrestrial broadcast channels", *Proc. IEEE Global Telecommunications Conf.*, vol. 1, pp. 1–5, 1994.

[6] D. Falconer, S.L. Ariyavisitakul, A. Benyamin-Seeyar, and B. Eidson, "Frequency domain equalization for single-carrier broadband wireless systems", *IEEE Communications Magazine*, vol. 40, pp. 58–66, April 2002.

[7] S.B. Weinstein and P.M. Ebert, "Data transmission by frequency division multiplexing using the discrete fourier transform", *IEEE Trans. on Communications*, vol. 19, pp. 628–634, Oct. 1971.

[8] L.J. Cimini Jr., "Analysis and simulation of a digital mobile radio channel using orthogonal frequency division multiplexing", *IEEE Trans. on Communications*, vol. 33, pp. 665–765, July 1985.

[9] J.A.C. Bingham, "Multicarrier modulation for data transmission: An idea whose time has come", *IEEE Communications Magazine*, vol. 28, pp. 5–14, May 1990.

[10] J.G. Proakis, *Digital Communications*, McGraw-Hill, New York, NY, 3rd edition, 1995.

[11] R.B. Yates and N.B. Mandayam, "Challenges in low-cost wireless transmission", *IEEE Signal Processing Magazine*, vol. 17, pp. 93–102, May 2000.

[12] D.D. Falconer and F.R. Magee, "Adaptive channel memory truncation for maximum likelihood sequence estimation", *Bell System Technical Journal*, vol. 52, pp. 1541–1562, Nov. 1973.

[13] S.N. Diggavi, "Analysis of multicarrier transmission in time-varying channels", *Proc. IEEE Intern. Conf. on Communication*, vol. 3, pp. 1191–1195, 1997.

[14] P. Robertson and S. Kaiser, "The effects of doppler spreads on OFDM(A) mobile radio systems", *Proc. IEEE Vehicular Technology Conference*, vol. 1, pp. 329–333, 1999.

[15] Y.H. Kim, I. Song, H.G. Kim, T. Chang, and H.M. Kim, "Performance analysis of a coded OFDM system in time-variant multipath rayleigh fading channels", *IEEE Trans. on Vehicular Technology*, vol. 48, no. 5, pp. 1610–1615, 1999.

[16] B. Stantchev and G. Fettweis, "Time-variant distortions in OFDM", *IEEE Communications Letters*, vol. 4, pp. 312–314, Oct. 2000.

[17] J. Ahn and H.S. Lee, "Frequency domain equalization of OFDM signals over frequency nonselective Rayleigh fading channels", *Electronics Letters*, vol. 29, pp. 1476–1477, Aug. 1993.

[18] L. Wan and V.K. Dubey, "Analysis of the demodulation techniques for OFDM signals under correlated Rayleigh fading", *Proc. IEEE Vehicular Technology Conference*, vol. 1, pp. 772–726, 2001.

[19] M. Russell and G.L. Stuber, "Interchannel interference analysis of OFDM in a mobile environment", *Proc. IEEE Vehicular Technology Conference*, vol. 2, pp. 820–824, 1995.

[20] J. Armstrong, P.M. Grant, and G. Povey, "Polynomial cancellation coding of OFDM to reduce intercarrier interference due to doppler spread", *Proc. IEEE Global Telecommunications Conf.*, vol. 5, pp. 2771–2776, 1998.

[21] Y. Zhao and S.-G. Haggman, "Intercarrier interference self-cancellation scheme for OFDM mobile communication systems", *IEEE Trans. on Communications*, vol. 49, pp. 1185–1191, July 2001.

[22] W.G. Jeon, K.H. Chang, and Y.S. Cho, "An equalization technique for orthogonal frequency-division multiplexing systems in time-variant multipath channels", *IEEE Trans. on Communications*, vol. 47, pp. 27–32, Jan. 1999.

[23] J.-P.M.G. Linnartz and A. Gorokhov, "New equalization approach for OFDM over dispersive and rapidly time varying channels", *Proc. IEEE Internat. Symposium on Personal, Indoor and Mobile Radio Communications*, vol. 2, pp. 1375–1379, 2000.

[24] Y.-S. Choi, P.J. Voltz, and F.A. Cassara, "On channel estimation and detection for multicarrier signals in fast and selective rayleigh fading channels", *IEEE Trans. on Communications*, vol. 49, pp. 1375–1387, Aug. 2001.

[25] X. Cai and G.B. Giannakis, "Low-complexity ICI suppression for ofdm over time- and frequency-selective Rayleigh fading channels", *Proc. Asilomar Conf. on Signals, Systems and Computers*, Nov. 2002.

[26] S. Verdu, *Multiuser Detection*, Cambridge, New York, 1998.

[27] N. Al-Dhahir, "FIR channel-shortening filters for MIMO ISI channels", *IEEE Trans. on Communications*, vol. 49, pp. 213–218, Feb. 2001.

[28] S.K. Mitra, *Digital Signal Processing*, McGraw-Hill, New York, NY, 2nd edition, 3001.

[29] R. Li and G. Stette, "Time-limited orthogonal multicarrier modulation schemes", *IEEE Trans. on Communications*, vol. 43, no. 2/3/4, pp. 1269–1272, 1995.

[30] M. Gudmundson and P.-O. Anderson, "Adjacent channel interference in an OFDM system", *Proc. IEEE Vehicular Technology Conference*, pp. 918–922, Apr. 1996.

[31] K. Matheus and K.-D. Kammeyer, "Optimal design of a multicarrier system with soft impulse shaping including equalization in time or frequency direction", *Proc. IEEE Global Telecommunications Conf.*, vol. 1, pp. 310–314, 1997.

[32] R.W. Lowdermilk and f.harris, "Design and performance of fading insensitive orthogonal frequency division multiplexing (OFDM) using polyphase filtering techniques", *Proc. Asilomar Conf. on Signals, Systems and Computers*, pp. 674–678, 1997.

[33] C. Muschallik, "Improving OFDM reception using adaptive Nyquist windowing", *IEEE Trans. on Consumer Electronics*, vol. 42, pp. 259–269, Aug. 1996.

[34] A.V. Oppenheim and R.W. Schafer, *Discrete-Time Signal Processing*, Prentice-Hall, Englewood Cliffs, NJ, 1989.

[35] W.C. Jakes, *Microwave Mobile Communication*, Wiley, New York, NY, 1974.

[36] H. Sari, G. Karam, and I. Jeanclaude, "Transmission techniques for digital terrestrial TV broadcasting", *IEEE Communications Magazine*, pp. 100–109, Feb. 1995.

[37] P. Davis, *Circulant Matrices*, Wiley, New York, 1979.

[38] G. Forney, "Maximum-likelihood sequence estimation of digital sequences in the presence of inter symbol interference", *IEEE Trans. on Information Theory*, vol. 18, no. 3, May 1972.

[39] L.L. Scharf, *Statistical Signal Processing: Detection, Estimation, and Time Series Analysis,*, vol. 1, Addision-Wesley, NY, 1991.

[40] Y. Zhou and G.B. Giannakis, "Finite-alphabet based channel estimation for OFDM and related multicarrier systems", *IEEE Trans. on Communications*, vol. 49, pp. 1402–1414, Aug. 2001.

[41] B. Muquet, M. De Courville, and P. Duhamel, "Subspace-based blind and semi-blind channel estimation for OFDM systems", *IEEE Trans. on Signal Processing*, vol. 50, pp. 1699–1712, July 2002.

[42] H. Bolcskei, R.W. Heath, and A.J. Paulraj, "Blind channel identification and equalization in OFDM-based multiantenna systems", *IEEE Trans. on Signal Processing*, vol. 50, pp. 96–109, Jan. 2002.

[43] H. Rohling, T. May, K. Bruninghaus, and R. Grunheid, "Broad-band OFDM radio transmission for multimedia applications", *Proceedings of the IEEE*, vol. 87, pp. 1778–1789, Oct. 1999.

[44] M. Lott, "Comparison of frequency and time domain differential modulation in an OFDM system for wireless ATM", *Proc. IEEE Vehicular Technology Conference*, vol. 2, pp. 877–883, 1999.

[45] R. Schober and W.H. Gerstacker, "Adaptive noncoherent linear minimum ISI equalization for MDPSK and MDAPSK signals", *IEEE Trans. on Signal Processing*, vol. 49, pp. 2018–2031, Sept. 2001.

[46] R. Schober and W.H. Gerstacker, "Noncoherent adaptive channel identification algorithms for noncoherent sequence estimation", *IEEE Trans. on Communications*, vol. 49, pp. 229–234, Feb. 2001.